NASA CONTRACTOR REPORT 166483

Feasibility Study of Three-Dimensional Holographic Interferometry for Aerodynamics

J.E. Craig

CONTRACT NAS2-10573
May 1983

NASA

NASA CONTRACTOR REPORT 166483

Feasibility Study of Three-Dimensional Holographic Interferometry for Aerodynamics

J.E. Craig
Spectron Development Laboratories Inc.
3303 Harbor Boulevard, Suite G-3
Costa Mesa, CA 92626

Prepared for
Ames Research Center
Under Contract NAS2-10573

National Aeronautics and
Space Administration

Ames Research Center
Moffett Field, California 94035

TABLE OF CONTENTS

1.0 INTRODUCTION

This report documents work conducted over a 2.5 year span which was primarily of a consulting nature. The work involved many aspects of holographic interferometry and specifically the feasibility of three dimensional measurement. The work was divided into six tasks described in Section 2.0.

Tasks I and II - the delivery of a literature survey and a tomography computer program.

Task III - a feasibility study of the use of alignment elements in the dual plate holographic interferometry.

Task IV - acquisition of oscillating airfoil data.

Task V - a feasibility study of three-dimensional holographic interferometry.

Task VI - an axisymmetric flow investigation.

2.0 TECHNICAL DICUSSION

2.1 Task I and II - Tomography Background

On June 17, 1980, a meeting was held between B.P. Hildebrand and George Lee and his staff at NASA Ames laboratory to discuss the various tomography algorithms available. Currently being tested is the Fourier transform algorithm developed by Bruechner at the Naval Post Graduate School. This algorithm is probably the most sensitive to missing data of all the algorithms used in the medical CAT machines. It was suggested that some of the iterative algorithms, such as ART or SIRT would be more suitable to this application.

A short literature survey was made and the most pertinent papers were left at NASA for copying. One paper, in particular, studies methods for circumventing the missing data problem by filling in with a smooth function fitted to the edges of the shadow. This method, coupled with the ART algorithm, should yield satisfactory results.

A tape containing ART as received from the Mayo Clinic in 1976 was sent to Mr. Jeff Trosin. A second program, TFTOM, for reconstruction of an image field was also forwarded to Mr. Trosin.

The computer programs were configured by Ames personnel.

2.2 Task III - Alignment Element

2.2.1 Purpose

An alignment element has been designed as an integral component of the double-plate holographic interferometer. The alignment elements produce additional interferograms which are utilized to adjust the double-plate interferometer into the infinite fringe configuration. The alternate interferograms are especially useful and are escentially required when high accuracy and repeatability are desired to when the optical disturbance fills the field of view.

2.2.2 Theory of Operation

The object beam is collimated between the Schlieren mirrors so that the rays are perpendicular to the U and V velocity planes within the wind tunnel test section. Hence, for two-dimensional flows the rays traverse constant property paths except near the wind tunnel windows where boundary layers are present. The test section windows and the object beam each have a diameter of 400 mm. A spherical phase error is introduced by attaching three small positive lenses to the wind tunnel window. These spherical waves pass throughout the holography system and are captured at the hologram plane as converging waves. The remainder of the object wave passes unobstructed through the test section and is recorded holographically in the usual manner.

Both holograms are recorded on the same physical location on the holographic plate and in reconstruction both sets of waves are produced.

In reconstruction, a spatial filter, 3 small pinholes located at the focal points of the alignment waves, is used to block the flow field waves from the flow-on and flow-off holograms. The alignment waves are diverging spherical waves beyond the spatial filter. With a screen placed within the three alignment waves, interference patterns will be observed. These interference patterns are produced by the overlapping of the flow on and flow off alignment waves produced by each of the three alignment elements. The double plate interferometer is adjusted until infinite fringe spacing is achieved within the alignment interference patterns. For such a condition, the flow field interferogram is then accurately positioned in the infinite fringe configuration. To photograph the flow field interferogram, the alignment wave spatial filter is removed and the flow field spatial filter installed. Thus blocking the alignment waves and allowing the flow interferogram to be photographed. The flow interferogram exhibits shadows of the AE's.

2.2.3 Design

The optical schematic (Figure 1) shows both the alignment element waves and usual flow field waves. The selected AE's are simple positive lenses with a 2 meter focal length and a 17 mm diameter. The AE's are placed at 120° spacings (4, 8, and 12 o'clock) at a radius of 90 mm on the test section window. The alignment waves are brought to a focus near the focal point of the east Schlieren mirror, and thus the alignment waves are collimated ($\phi \sim 25$ mm) between the mirror and the lens ($F' = 500$ mm, $\phi' = 100$ mm). The lens converges the alignment waves toward the hologram where they are recorded at 12 mm diameter.

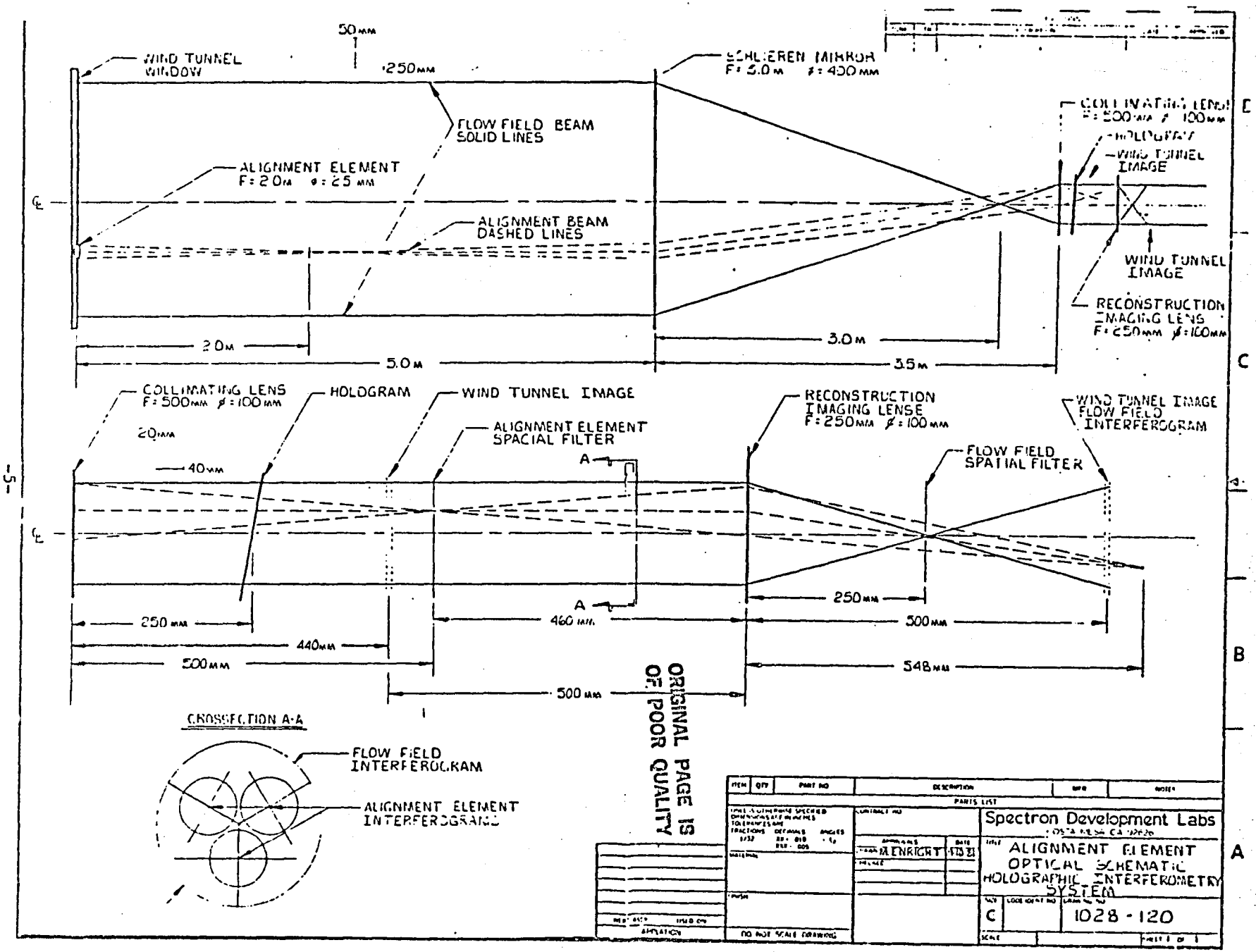

FIGURE 1. ALIGNMENT ELEMENT - OPTICAL SCHEMATIC - HOLOGRAPHIC INTERFEROMETRY SYSTEM

In reconstruction, both alignment and flow field waves are produced. Initially, the alignment waves are spatially filtered and course interferometer adjustment is achieved by overlapping physical objects within the test section such as the airfoil, the AE's, or the edge alignment pins at 3, 6, and 12 o'clock positions. The interferometer must be adjusted to course alignment before interference fringes of detectable spacings are produced within the alignment interferograms. Since the alignment interferograms are very sensitive to interferometer adjustment, interference fringes will not have a resolvable spacing (say 300 μ) until the plates are repositioned within 0.5 mm.

The spherical alignment waves produce interference patterns when their centers of curvature are misaligned. The interferogram fringe spacing is uniform when the double-plate interferometer is near alignment. As alignment is approached, the fringe spacing broadens, and with a fringe spacing equal to the interferogram dimension, 20 mm, the transverse misalignment, Δ, of the center of curvature is

$$\Delta = \frac{\mu R}{S} = 7.5 \ \mu m$$

where λ : laser wavelength (0.5 μm)

R: alignment wave radius of curvature (300 mm)

S: fringe spacing.

The double-plate interferometer can in theory be adjusted to within at most 7.5 μm of perfect realignment.

2.3 Task IV - Oscillating Airfoil Experiment

The oscillating airfoil experiment was supported during May and June 1981. Previous to this test the holography system (Ref. 1) had never been synchronized to an externally triggered event, and holograms had been recorded at random times chosen by the system operator. Modifications were required to synchronize the laser clock to an external time base, namely the airfoil oscillator. Thus enabling the flow-on and flow-off holograms to be recorded at reproducible airfoil positions, especially during operation of the selected frequencies of operation (typically between 10 and 40 Hz). A large number of holograms were recorded throughout the test matrix of Mach numbers and airfoil oscillation (mean angle of attack, oscillation amplitude and frequency) parameters. Two goals were accomplished; (1) to acquire sufficient data to produce infinite fringe interferograms of the basic test matrix conditions, and (2) at one airfoil operating condition, holograms were recorded at closely spaced angles of attack ($\Delta\alpha$ = 1.25 degrees) for the purpose of constructing a one cycle movie. To monitor the quality of the data, about one third of the interferograms constituting the basic test matrix were produced during the period of data acqusition.

After the data acquisition, Ames personnel filed and documented the entire set of holograms, over 500 in number. Some double plate alignment and interferogram photography was performed.

This work has been published (Ref. 2) and a copy is included as Appendix 2.

2.4 Task V - Applied Tomography Measurements

Three-dimensional holography concepts are being investigated. Data acquisition occurred during two wind tunnel entries; (1) subsonic data in January 1981 and (2) supersonic data in November 1981. A hemispherical cylinder was chosen for the subsonic flow model for which the flow field can be accurately predicted. Flow Mach numbers of 0.6 and 0.8 were selected. The model was positioned as near as possible to the zero degree angle of attack for the initial tests. Then the model was rotated to 5 degrees angle of attack for the tomography holograms. The three-dimensional flow field is rotated through the holograph viewing direction in ten degree increments. Because of flow symmetry only 90 degrees of the 360 degrees of available views are unique.

Holograms were recorded at ten positions between and including 0 and 90° rotation about the flow direction. Twenty reconstructed holographic interferograms are required to complete both 0.6 and 0.8 Mach number test conditions. For a second phase of the effort, the hemispherical cylinder was extended forward to the window center and the data repeated. Twenty interferograms were obtained at this forward position and compared with data obtained in the rear position of the window.

A major problem in this experiment is the freestream turbulence within the wind tunnel. The turbulence is random in each view and acts to increase the noise in the phase profiles. The phase object in these experiments contained a signal level of about 5-10 waves and the

turbulence contains a phase of about 1 wave; hence the signal/noise is at most about 10. The turbulence noise level also complicates fringe numbering for infinite fringe alignment. Hence finite fringe alignment is recommended with about 30-50 fringes within the flow object.

A considerable number of holograms have already been recorded and another tunnel entry is required to finalize the hologram recording task. Upon completion of double-plate alignment and interferogram photography tasks, a complete set of multiple view interferogram data will exist for a number of axisymmetric and three dimensional flow objects. Interferogram fringe measurement is required to produce phase profiles compatible with computer processing. The phase profile represent the raw data for the computer, and for these flow objects considerable attention must be paid to noise present within the signal. The tomography program requires that additional constraints be met. The integral of the phase profile must be invariant with viewing angle. The missing portions of the phase profiles caused by model shadows must be inserted into the data. Finally, multiple view data can be inverted with the tomography code and density contours produced within a cross-section of the flow.

2.5 Task VI - Axisymmetric Flow Investigations

This work has been reported in an earlier document (SDL No. 82-2152-14DF, April 1982), which is included in Appendix 1.

3.0 SUMMARY AND RECOMMENDATIONS

3.1 Task IV - Oscillating Airfoil

A large amount of very interesting transonic flow data was recorded in the oscillating arifoil experiment under the direction of Don Buell. During Phase I of the experiment, holography data wa acquired. Many aspects of the phenomena of dynamic s*all were, for the first time, quantitatively resolved with holographic interferometry. The dynamics of turbulent separation and particular flow hysteresis during airfoil oscillation was graphically visualized.

We propose to review and complete single- and double-plate reconstruction efforts. The interferograms should be carefully reviewed with the Project Engineer, Don Buell, and appropriate conditions selected for evaluation. Fringe measurements should be obtained and interpreted. Data should be compared with other measurements, (LDV and pressure) and/or numerical flow field calculations. A detailed description of the work should be prepared and published jointly with Ames in journa literature.

3.2 Task V - 3-D Holography

Three dimensional holography concepts are being investigated experimentally. Two major objectives were accomplished in the investigation. Computational capability to invert multiview data to give cross-sectional distributions of density was obtained and is operational on the Ames Computer Facility. The code uses the FFT inversion technique. Experimental data has been acquired at transonic flow speeds to

evaluate the code capability to withstand noise, opaque objects, and limited number of views. This data is of high quality and should be used to scrutinize and evaluate various inversion codes.

We propose to review and complete double-plate alignment, interferogram photography, fringe measurement and computer inversion of the multiple view interferogram data. The effect of turbulence or noise, shadows, and finite viewing angles on the inversion quality would be assessed for the FFT and other (ART) inversion codes. This new and important work will be published jointly with Ames in a journal publication.

3.3 Task VI - Axisymmetric Bump

Flow measurements of axisymmetric shock wave boundary layer interactions in transonic flow have been obtained using holographic interferometry. The flow Mach number was varied from 0.8, where only weak pressure waves are present to 0.925, well above the Mach number, where the shock wave induces separation. In the earlier experiments performed in the 2x2 foot wind tunnel the interferogram field of view did not extend into the undisturbed flow. In the current experiments the model positioned in three locations with respect to the viewing window ($x = 256$ mm and $y = 356$ mm, where the streamwise direction, x, and cross-stream direction, y, are introduced) providing visualization of about three times the field in the cross-stream direction ($y/t = 34.5$, where the maximum bump thickness, t, is introduced). Hence using composite interferograms from the three fields of view, the quantitative

visualization will extend well into this undisturbed portion of the flow field.

Interferograms should be produced which encompass the disturbed flow. For Mach numbers above 0.85, this requires combining interferograms at two or possibly three positions. For a few selected cases, fringe measurement and Abel inversion should be attempted. If the preliminary inversion attempts are promising, we would propose to invert the complete flow fields for all five Mach numbers, and prepare pressure or Mach number contours. Advanced techniques utilized for tomographic inversion would also be investigated. Of particular interest is the rejection of noise by filtering in the spatial or frequency domain.

4.0 REFERENCES

1. Craig, J. E., Lee, G., and Bachalo, W. D., "An Nd:YAG Holographic Interferometer for Aerodynamic Research", presented at the 26th International SPIE Technical Symposium, San Diego, California, August, 1982.

2. Lee, G., Buell, D. A., and Licursi, J., "Laser Holographic Interferometry for Unsteady Airfoil Undergoing Dynamic Stall", AIAA-83-0388, AIAA 21st Aerospace Sciences Meeting, Reno, Nevada, January 10-13, 1983.

APPENDIX 1

FLOW MEASUREMENTS OF AXIALLY SYMMETRIC SHOCK WAVE BOUNDARY LAYER INTERACTIONS WITH HOLOGRAPHIC INTERFEROMETRY

(SDL No. 82-2152-14DF - April 1982)

FLOW MEASUREMENTS OF AXIALLY SYMMETRIC SHOCK WAVE BOUNDARY LAYER INTERACTIONS WITH HOLOGRAPHIC INTERFEROMETRY

DRAFT FINAL REPORT

James E. Craig
and
William D. Bachalo

SDL No. 82-2152-14DF

April 1982

Prepared For:

NASA AMES RESEARCH CENTER
Moffett Field, California 94035

Under Contract:

NAS2-10573

3303 Harbor Boulevard, Suite G-3
Costa Mesa, California 92626 (714) 549-8477

TABLE OF CONTENTS

ABSTRACT

Shock wave boundary layer interactions in transonic flows have been investigated on an axisymmetric flow model using holographic interferometry. The current experiment was motivated by previous research conducted with the same model in the 2x2 foot wind tunnel. On the earlier program comprehensive LDV measurements were obtained in the separation region; however, questions regarding wall interference motivated the use of a large wind tunnel. The objectives were the determination of quantitative data on the inviscid density profiles and to qualitatively evaluate shock wave stability. Double plate holographic interferometry was used to obtain fringe data which requires Abel integration to obtain density profiles. Double pulse interferograms did not reveal discernable shock wave motion for laser pulse spacings up to 300 μs.

Initial double-plate reconstruction efforts revealed excellent fringe contrast. Alignment of the double-plate holographic interferometer to the infinite fringe configuration could not be performed accurately because the window aperture did not extend beyond the flow disturbance. A second factor which hindered interferometer alignment was vibration along the long optical path (100 ft). Alignment accuracy can be determined by inventing the fringe position data to density profiles, and comparing the density at the model surface to values determined from surface pressure measurements. It seems that some iteration between interferometer alignment and Abel inversion would be necessary. Initial reconstruction appears to be an adequate starting point.

1.0 INTRODUCTION

Shock wave boundary layer interactions in transonic flows have been investigated on an axisymmetric flow model using holographic interferometry. The model concept is patterned after that of Roshko and Thomke (Ref. 1) who utilized an annular wedge affixed to a hollow circular cylinder aligned with the flow direction. The hollow tube is sufficiently long that natural transition occurs and quasi 2-D interactions can be generated and studied in the absence of edge effects. For these tests, at transonic flow speeds, a circular arc bump was attached to a circular cylinder. The bump was located at a point along the tube where the boundary layer was already turbulent and in addition, thick enough that its characteristics could be determined. The axisymmetric model shape allows laser velocimetry probing very close to the wall. Such experiments have been conducted in a previous research program in the 2x2 foot wind tunnel (Ref. 2) and produced many important details of the shock induced turbulent boundary layer separation in the transonic speed range. Holographic interferograms were also recorded. However, the interpretation of these data was hampered since the model disturbance extended to the wind tunnel walls. A set of experiments were conducted in the 6x6 foot wind tunnel to investigate the question of wall effects and shock stability. The flow field about the axisymmetric model was assumed to be without wall effects in the larger facility. For these initial experiments surface pressure data and holographic interferograms constitute the data.

The primary test objectives were the determination of quantitative data in the inviscid density distribution and to qualitatively evaluated

shockwave stability. Double plate holography was used to obtain flow interferograms.

The freestream Mach number was varied from 0.8, where only weak compression waves are present, to 0.925, well above the Mach number for shock induced boundary layer separation. Single pulse flow holograms were recorded at five freestream Mach numbers and three model positions (Table 1). Flow-off holograms required for the double plate interferometer were recorded with the model in view, position A, and, with the model out of view, position C. The holograms were reconstructed with and without an aligned reference (no flow) plate in a reconstruction system designed to reproduce the construction reference wave. Shadowgrams and interferograms were photographed and are presented in the results section. Analysis of the fringe data will take advantage of the axisymmetric flow geometry. Density distributions may be estimated from Abel type integrations of the fringe data; however, the presence of freestream turbulence and interferometer errors can destabilize the Abel process. Iterative techniques used in multi-view tomographic reconstruction are much less sensitive to these error sources.

Shockwave stability was investigated with double pulse holographic interferometry which is sensitive to time variations in density. Fringe activity within the double image of the shockwave constitutes the primary data. Fringes in the inviscid flow and the separated zone are also possible. Holograms were recorded with pulse spacings of 30, 100 and 300 us, with the model in positions A and C, and for a flow Mach number of 0.875. The holograms were reconstructed and photographed.

2.0 THE EXPERIMENT

2.1 Model

The interaction is induced on the outer surface of a 150 mm diameter circular cylinder. A smooth circular arc bump extends from the 610 mm to the 810 mm station, Figure 1. The bump thickness, 19 mm, is sufficient to produce a critical flow Mach number of 0.8. The shock induced separation was produced on the recompression portion of bump.

Earlier experiments in the 2-Foot Transonic Wind Tunnel revealed the lack of undisturbed flow within the available field of view which extended to $y/t = 12$. The questions of model blockage in the small tunnel also motivated the tests in the larger test section.

Unfortunately, the 2-foot diameter windows proposed for the experiments apparently never existed and a smaller rectangular window (250 mm x 350 mm) was substituted. However, in the larger cross section wind tunnel, the model could be traversed in the cross stream direction to obtain interferograms extending well into the undisturbed flow ($y/t = 36$). Three model positions were used in the tests as shown in Figure 2, which also illustrates the available field of view obtained in the 2-foot experiments. In position A, only the bump portion of the model is visible in the bottom of the window; for positions B and C, the model is completely out of view.

2.2 Holographic Interferometer

A holographic interferometer system used in an earlier AFWL test program in the 6-foot wind tunnel was modified for the purpose of constructing double plate holographic interferograms (Figure 3). The system is constructed around a pulsed ruby laser built by Spectron for the AFWL. The laser is mounted on a large plate upon which the beamsplitter and object and reference beam spatial filter assemblies are also mounted. The object beam is directed into the primary Schlieren mirror which collimated the beam, directs it through the wind tunnel test section, and into the receiving Schlieren mirror. The receiving Schlieren mirror directs the converging object beam into the hologram where it is recorded with a dimension of 44 mm x 63.5 mm. The reference beam was collimated at a dimension of 25 mm and directed along the object beam path. The reference beam is passed over the test section instead of through it.

The reference beam was collimated at 100 mm diameter at the receiving stage and directed at the hologram. The normal to the hologram was not centered between the object and reference beams, but was skewed towards the reference beam. The object/reference beam angle was about 30 degrees.

Holograms were recorded with the room lights off and the room windows covered. Flow-off holograms were recorded in the conventional manner with the spacer removed from the film back. Flow-on holograms were recorded with the spacer in place. Double pulse holographic interferograms were recorded of pulse spacings of 30, 100, and 300 μs. The system was operated by one person at the receiving station and one at the laser.

3.0 RECONSTRUCTION

The primary objective of the experiment was to obtain double plate holographic interferograms of the shock boundary layer interaction. A double plate reconstruction system was designed and assembled in the SDL Holography Laboratory as shown in Figure 4. The design incorporated the optical parameters utilized for hologram recording, including the use of the AFWL collimating lense. The double plate holder was positioned within the reconstruction beam and adjusted to the recording angle. The reconstructed object waves were directed between two mirrors and collimated at 2 x 3 inch format. The 5 x 5 inch camera back was placed at the wind tunnel focal plane and reconstructed images were recorded on Kodak Tri-X film.

3.1 Results

The holograms were reconstructed and inspected for quality (brightness, uniformity, multimolding, etc.) Almost all of the holograms exhibited striking diffraction efficiencies, and about half of the holograms reconstructed uniform images without multimoding modulation. However, it was observed that the focal spot position of the reconstructed waves varied as much as a quarter of an inch. This is a strong indication of recording system vibration.

Single and double pulse flow on holograms were photographed directly. Initial attempts to align the double plate interferometer to infinite fringe revealed that the model images from the flow-on and flow-off plates were considerably displaced. Alignment pins were also

displaced. The degree of displacement varied for different flow-on (#'s 5-30) and flow-off holograms (#'s 1-4 and 31-34). The displacement in the infinite fringe images has the effect of terminating the interferogram before it reaches the model surface (i.e., only the flow-on shadowgram image is seen in the non-overlapping region). To extend the interferogram to the model surface in the flow-on hologram, the flow-off holograms, #'s 31-34, recorded in the absence of the model were used.

4.0 DISCUSSION

Flow shadowgrams and interferograms recorded at positions A-C are presented in Figures 5-9 for Mach numbers 0.80 through 0.925, respectively. Mach number comparisons of position A are presented in Figures 10 and 11. Double pulse interferograms at Mach number 0.875, recorded at positions A and C, are presented in Figures 12-14 for pulse spacings of 300 μs, respectively. Pulse spacing comparison is presented in Figure 15.

4.1 Inviscid Flow

Shock waves are propagated from the model surface at the 54 percent chord station for a Mach number of 0.80, and at the 63 ± 2 percent chord station for the higher Mach numbers. For the low Mach number (M = 0.8) case, the shock is normal to the bump surface. Shock wave curvature is observed near the surface for increasing Mach number. The extent of the curvature is increased further into the inviscid flow for increasing Mach number.

The apparent triangular shock wave image is an anomaly attributable to the axisymmetric geometry. The shock trajectory actually extends along a single path in a vertical cross section containing the model axis. The shock leaves the mode/surface sloping downstream but with curvature in the upstream direction. At larger radii the shock becomes perpendicular to the flow and remains so to much larger radii. Note that only within this vertical cross section are the light rays tangent to all points along the shock surface; whereas in other planes, the light rays are tangent only along portions of the shock surface

which are also perpendicular to the flow direction. The apparent intersection of the shock surface model surfaces which form the rearward leg of the triangle is actually formed by the shock surface at large radii in other circumferential planes. Thus, light rays appearing within the triangular shock region have intersected the curved portion of the shock at an oblique angle in some other circumferential plane (non-vertical).

Analysis of the fringe data will require some creative iteration between the double plate alignment and the fringe conversion calculation. It appears that the field of view extends to the zero fringe (qualitatively) for position A and Mach numbers to 0.875; whereas, for higher Mach numbers, the flow disturbance extends into the view, position C. The field of view is also limited in the flow direction to just beyond the ends of the circular arc bump (bump length 200 mm, window dimension 250 mm). For the higher Mach number cases, the interferogra.. record in positions A, B, and C and will have to be joined.

4.2 Shock Wave Stability

Double pulse interferograms are presented in Figures 12 through 15. The double pulse technique was selected to detect shock wave oscillation. Decker (Ref. 3) at NASA Lewis has used this technique to study shock waves in a transonic compressor rotor. For these experiments, two types of fringe information are observed; one depicting shock motion between pulses, and the other depicting the flow of freestream turbulence within the tunnel. The time between pulses can be adjusted to remove effects of slow moving phase objects. Note the increase in the turbulence fringes as the pulse spacings increased (Figure 15). For the longest pulse spacing (300 μs) the shock and the turbulence are readily

observed; however, double images of the shock are not observed. If the shocks observed in Figure 13 are superimposed, a displacement is observed ($\Delta \approx 10$ mm); however, position of the shock on the model surface is unchanged. Hence, it seems that, at most, only very small displacements in the shock position at the model surface occur while the shock position within the inviscid flow is unsteady.

Since the flow downstream of the shock wave is subsonic, acoustic disturbances within the separated shear layer can propagate upstream to the shock. Acoustic disturbances at the shock foot are quickly felt along the shock front; such disturbance are common in shock wave interactions with turbulent boundary layers. A final source of distortion is shock interaction with wind tunnel turbulence, which, for transonic speeds, includes fairly large pressure as well as velocity fluctuations.

5.0 CONCLUSIONS

Double plate holographic interferometry has been used to investigate axisymmetric flows. Infinite fringe plate alignment was only subjectively achieved because of excessive vibration in the hologram recording system. For the lower Mach number cases ($M \leq 0.875$), a single view of the flow was sufficient to span the inviscid flow field. The edge of the inviscid flow is blurred by freestream turbulence and errors in plate alignment. For high Mach number cases, the upper view interferograms must be joined to those with the model in view in order to reach the freestream. It would seem that some iteration between plate alignment and Abel inversion will be required, because of the subjective nature of the plate alignment.

6.0 REFERENCES

1. A. Roshko and G. J. Thomke, "Flare-Induced Interaction Length in Supersonic, Turbulent Boundary Layers," AIAA JOURNAL, Vol. 14, No. 7, pp 873-879, July 1976.

2. W. D. Bachalo and D. A. Johnson, "An Investigation of Transonic Turbulent Boundary Layer Separation Generated on an Axisymmetric Flow Model," AIAA 12th Fluid and Plasma Dynamics Conference, 79-1479, Williamsburg, Virginia, July 23-25, 1979.

3. Arthur J. Decker, "Holographic Flow Visualization of Time-Varying Shock Waves," APPLIED OPTICS, Vol. 20, page 3120, September 15, 1981.

TABLE 1. Hologram Log Sheet

DATE	TIME	HOLO #	MACH #	MODEL POSITION	TIME SPACING	
9/10/81	9:00	1-4	No Flow	Z = 0"	Sgl. Pulse	
	9:15	5-8	0.8	Z = 0"		
9/11/81	4:50	1-4	No Flow	Z = 0"	Sgl. Pulse	
9/11/81	5:10	5-6	0.85	Z = 0"		
9/11/81	5:15	7-10	0.875	Z = 0"		
9/11/81	5:20	11-12	0.90	Z = 0"		
9/11/81	5:25	13-14	0.925	Z = 0"		
9/11/81	5:34	15-16	0.925	Z = 6"	? May Not Have Been on	
9/11/81	5:38	17-18	0.90	Z = 6"	Condition for #15	
9/11/81	5:50	19-22	0.875	Z = 6"		
9/11/81	5:55	23-24	0.85	Z = 6"		
9/11/81	6:05	25-26	0.875	Z = 12"		
9/11/81	6:10	27-28	0.90	Z = 12"		
9/11/81	6:15	29-30	0.925	Z = 12"		
9/11/81	6:25/ 6:45	31-34	No Flow			
	Change to DBL Pulse					
9/11/81		35	0.875	Z = 12"	100 µs	2nd
9/11/81		36	0.875	Z = 12"	100 µs	both
9/11/81		37	0.875	Z = 12"	300 µs	both
9/11/81		38	0.875	Z = 12"	300 µs	1st
9/11/81		39	0.875	Z = 0"	300 µs	2nd
9/11/81		40	0.875	Z = 0"	300 µs	both
9/11/81		41	0.875	Z = 0"	300 µs	both
9/11/81		42	0.875	Z = 0"	300 µs	both
9/11/81		43	0.875	Z = 0"	100 µs	both
9/11/81		44	0.875	Z = 0"	100 µs	both
9/11/81		45	0.875	Z = 0"	100 µs	both
9/11/81		46	0.875	Z = 0"	100 µs	both
9/11/81	7:25	47	0.875	Z = 0"	30 µs	2nd
9/11/81		48	0.875	Z = 0"	30 µs	both
9/11/81		49	0.875	Z = 0"	30 µs	both
9/11/81		50	0.875	Z = 0"	30 µs	2nd

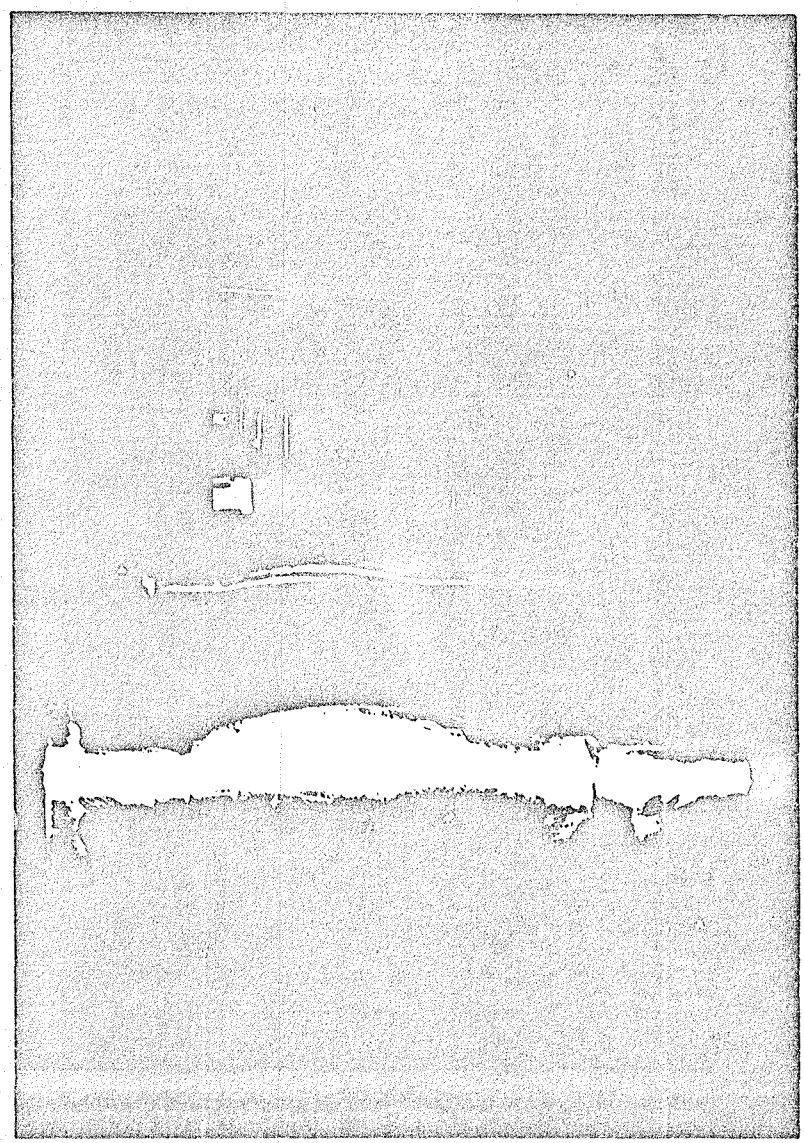

FIGURE 1. Axisymmetric Bump Model Installation
(Flow from Right to Left)

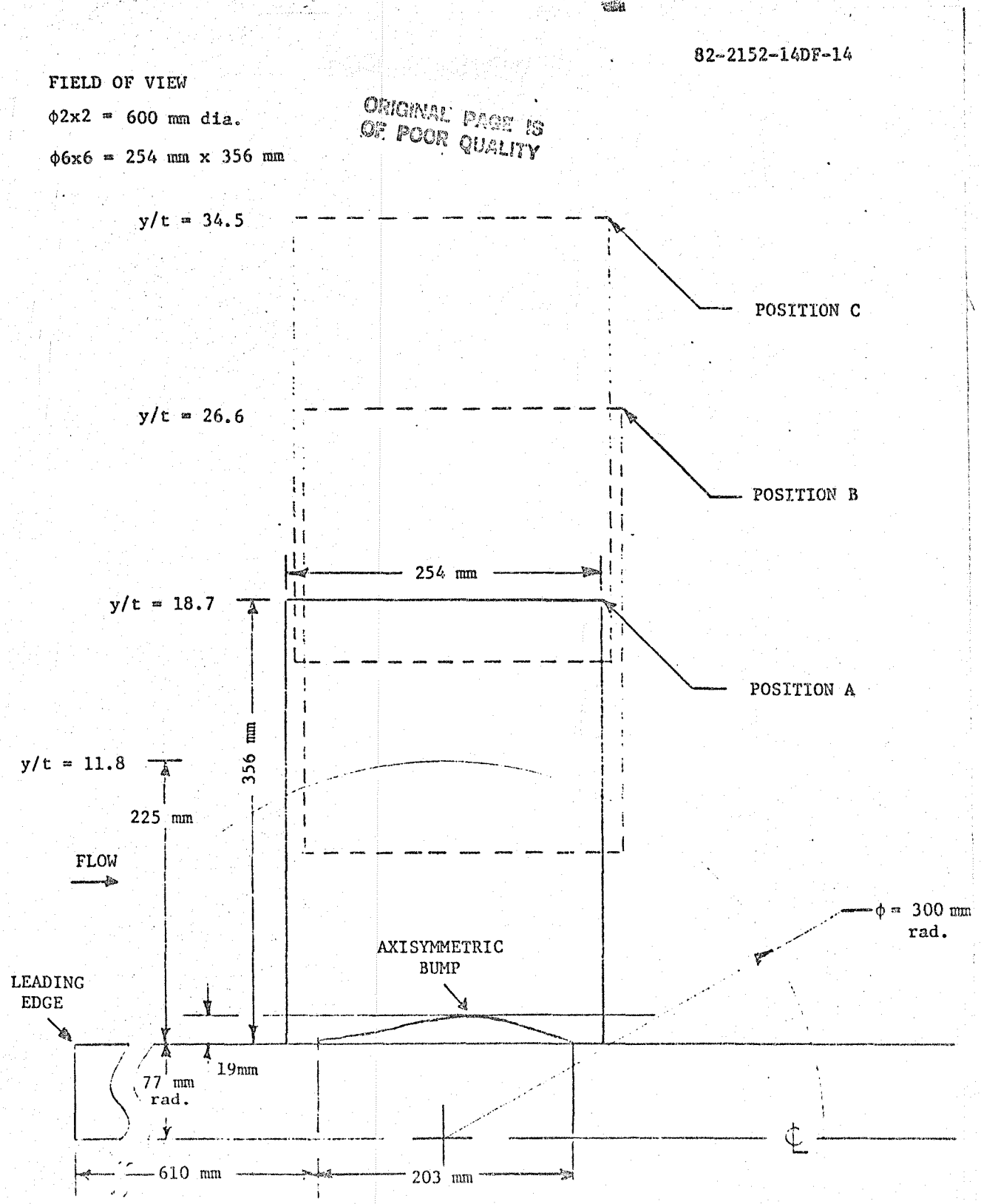

FIGURE 2. Comparison of Field of View Positions in 6x6 and 2x2 Foot Wind Tunnel Experiments

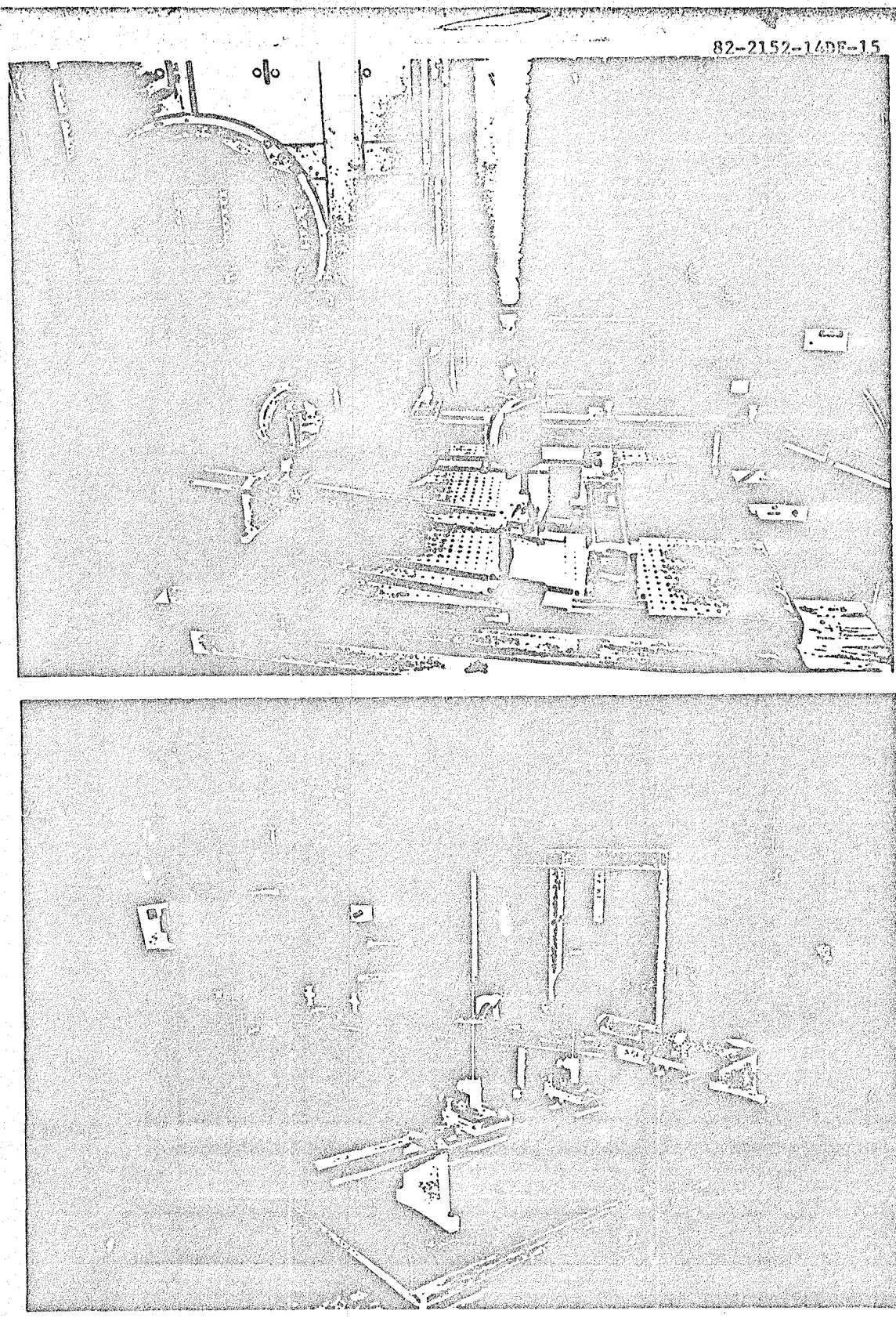

FIGURE 3. AFWL Pulsed Laser Holographic Interferometer Installation in 6x6 Foot Wind Tunnel
A) Transmitter and B) Receiver

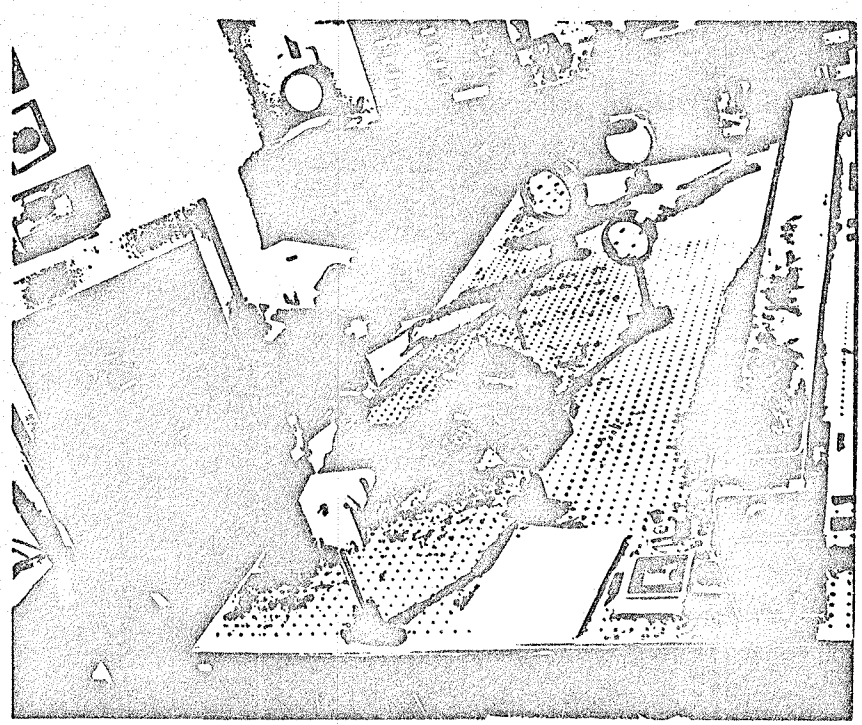

FIGURE 4. Spectron Reconstruction Laboratory

Model Position A

0: 6, 9/10

(Flow from Right to Left)

FIGURE 5. Shadowgram and Interferograms
Mach Number = 0.80
Reference Plate: 4, 9/10/81

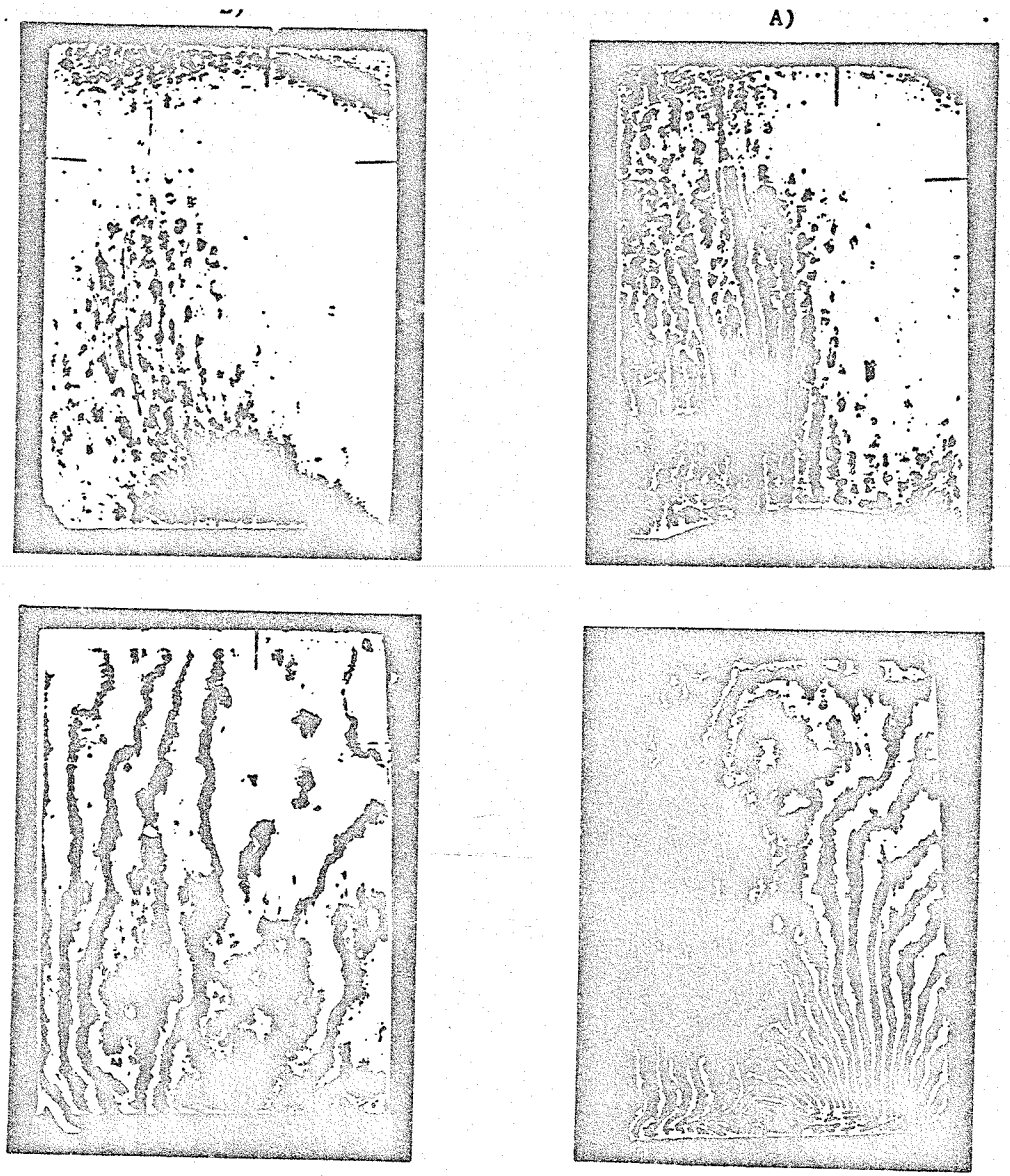

0:23, 9/11/81

0:5, 9/11/81 (Flow from Right to Left)

FIGURE 6. Shadowgram and Interferogram
Flow Mach Number = 0.85
Reference Plate: 33, 9/11/81

Model Position C) B) A)

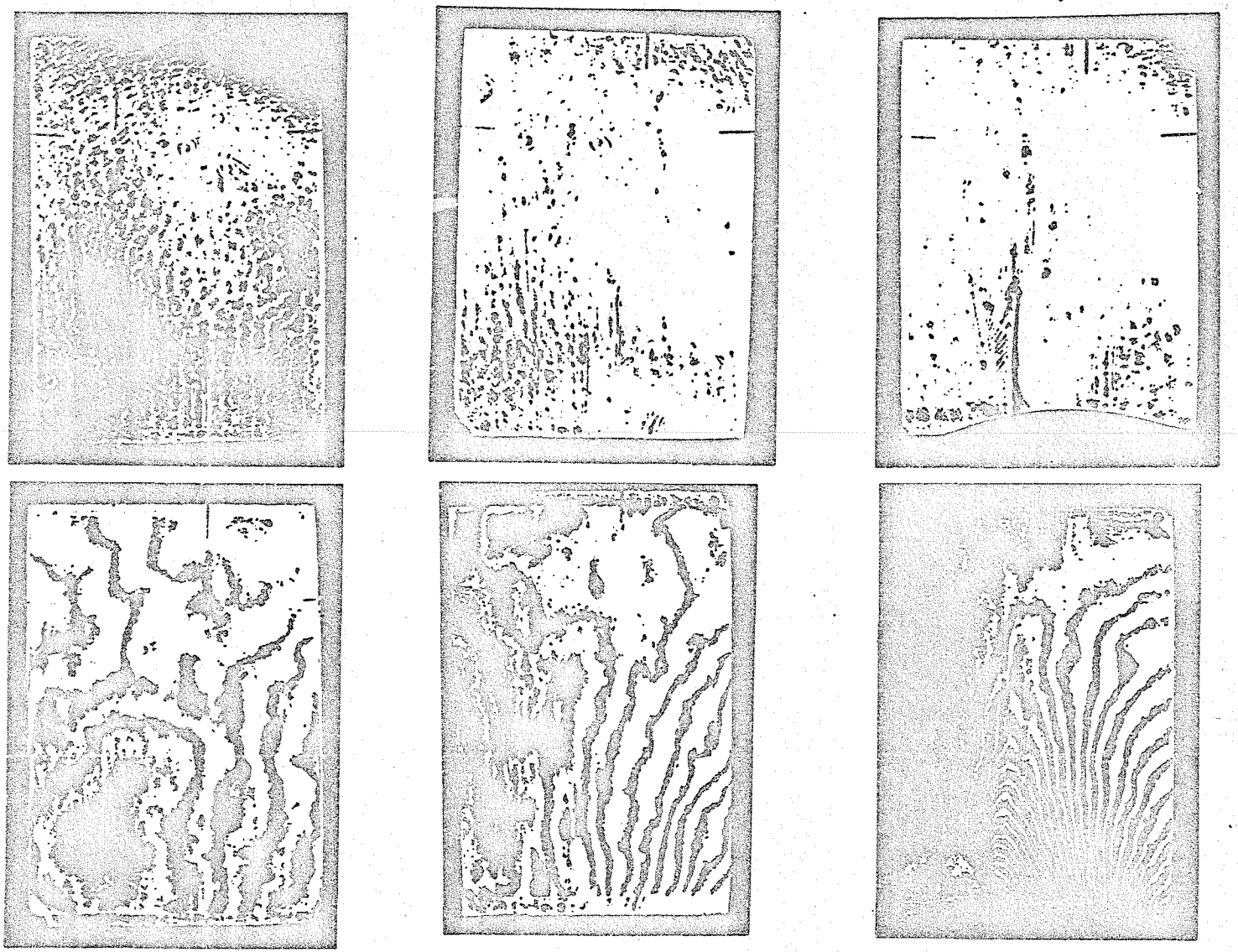

0:26, 9/11/81 0:21, 9/11/81 0:10, 9/11/81

FIGURE 7. Shadowgram and Interferogram
Flow Mach Number = 0.875
Reference Plate: 33, 9/11/81

(Flow from Right to Left)

el Position

C)

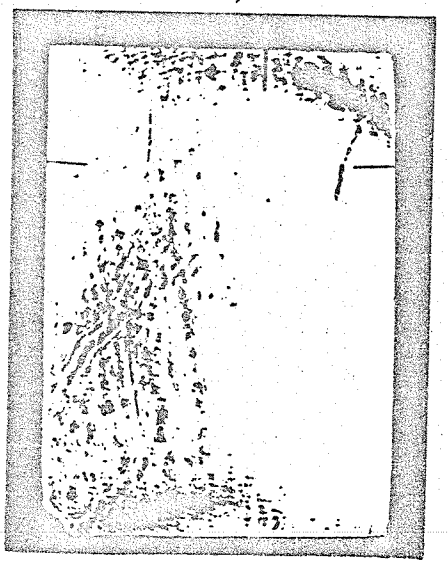

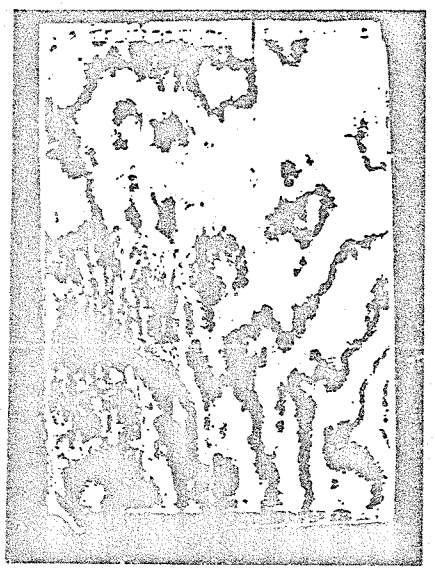

0:28, 9/11/81

B)

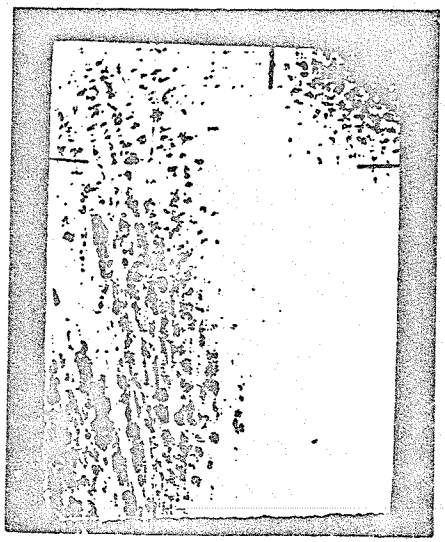

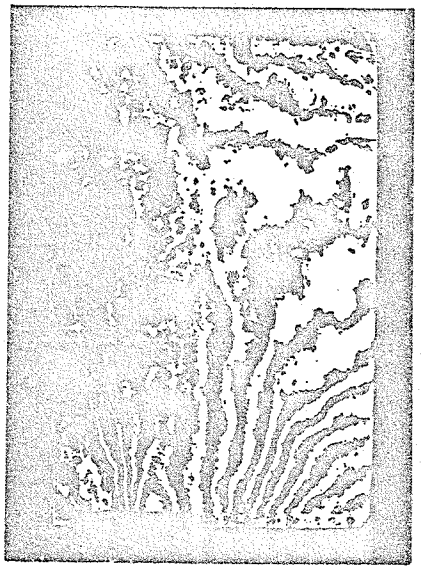

0:17, 9/11/81

A)

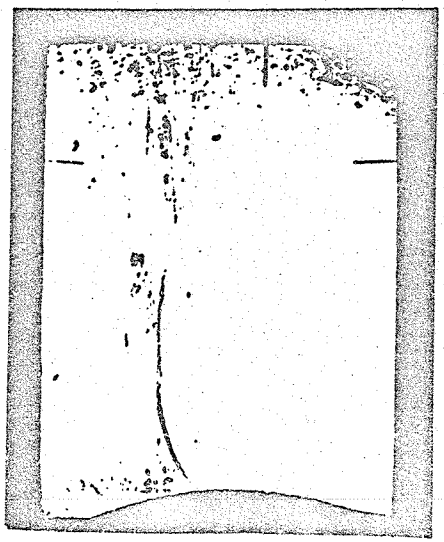

0:11, 9/11/81

FIGURE 8. Shadowgram and Interferograms
Flow Mach Number = 0.90
Reference Plate: 33, 9/11/81

(Flow from Right to Left)

del Position

C)

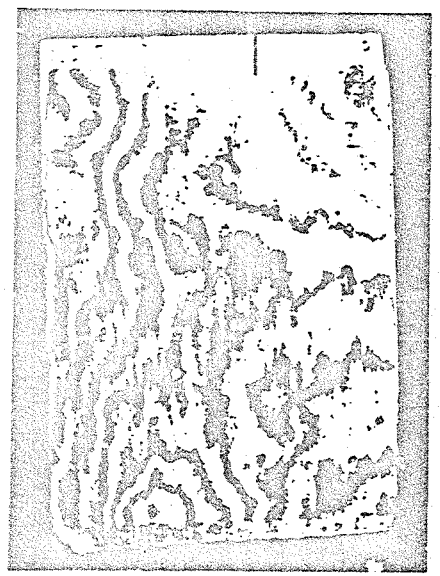

0:29, 9/11/81

B)

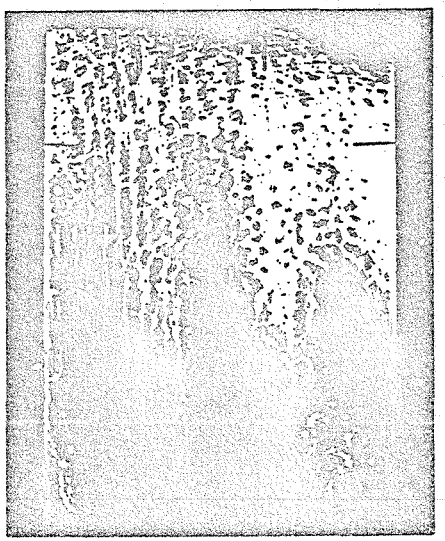

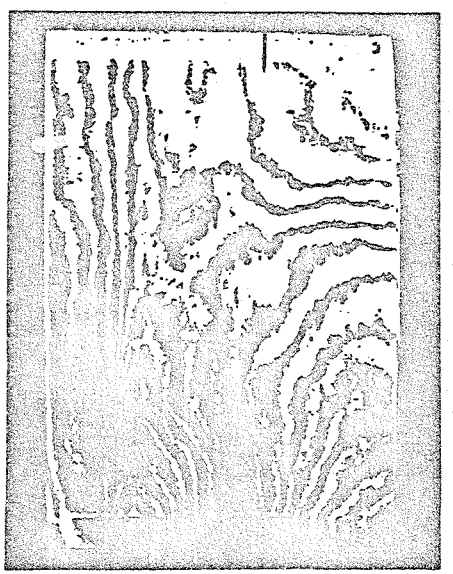

0:16, 9/11/81

A)

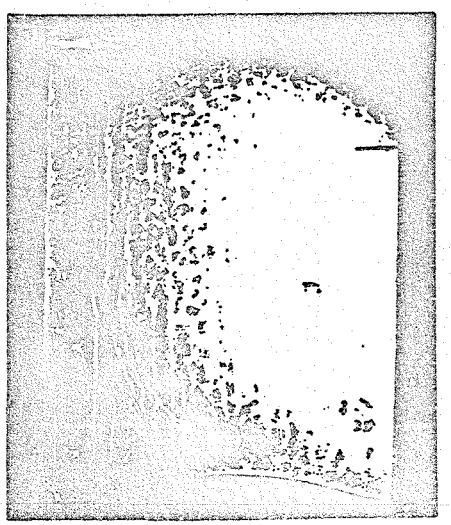

0:14, 9/11/81

(Flow from Right to Left)

FIGURE 9. Shadowgram and Interferogram
Flow Mach Number = 0.925
Reference Plate: 33, 9/11/81

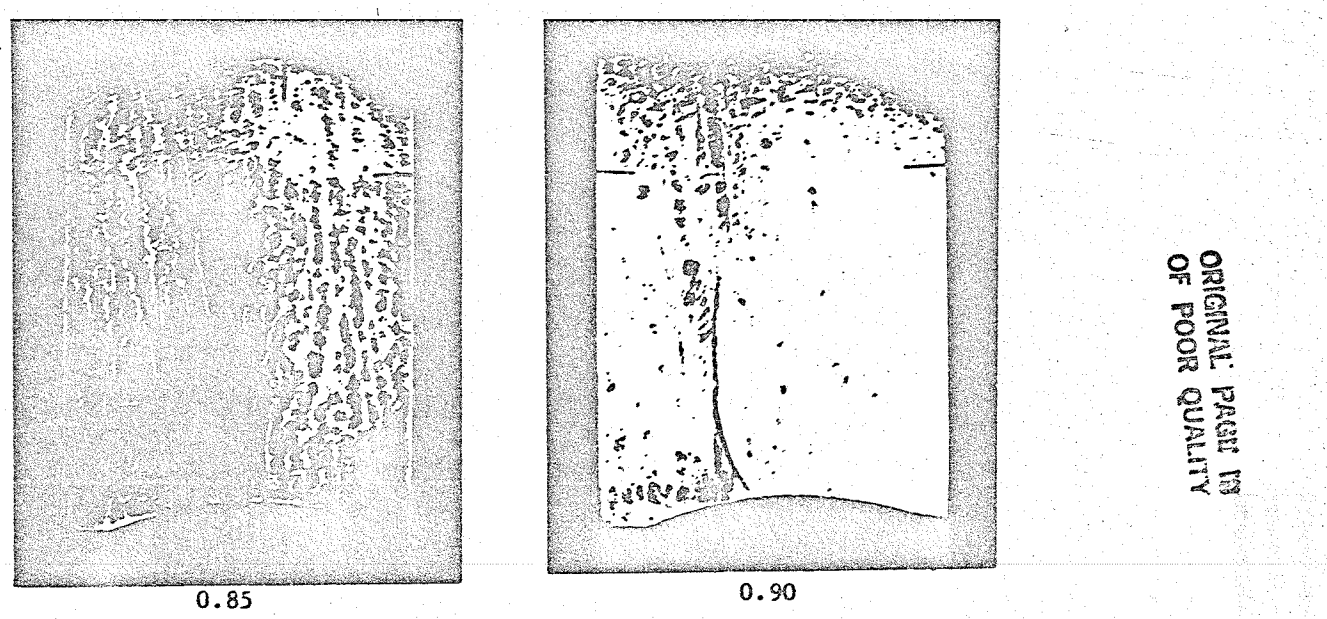

FIGURE 10. Shadowgram: Mach Number Comparison
Model Position A
(Flow from Right to Left)

FIGURE 11. Double Plate Holographic Interferograms: Mach Number Comparison
Model Position A. (Flow from Right to Left)

Model Position C

Hologram Number 37

Model Position A

Hologram Number 40

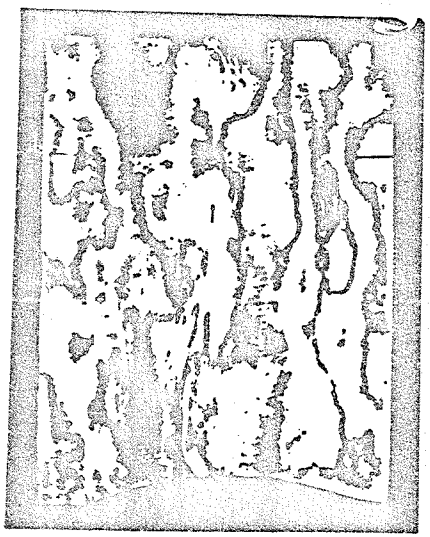

41

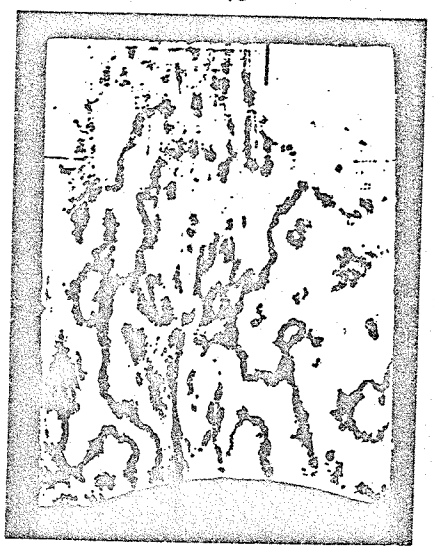

42

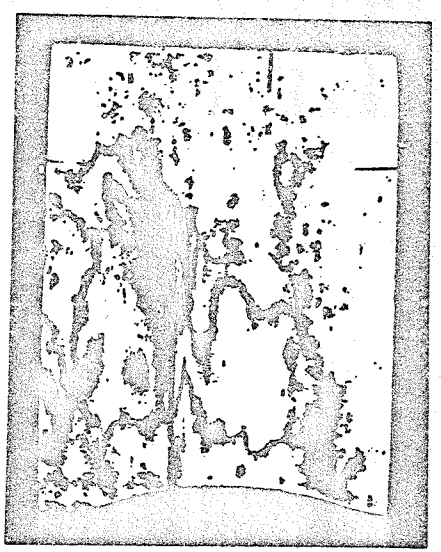

FIGURE 12. Double Pulse Holographic Interferograms: Flow Mach Number 0.875 Pulse Spacing 300 μs. (Flow from Right to Left)

Model Position C

Hologram Number 36

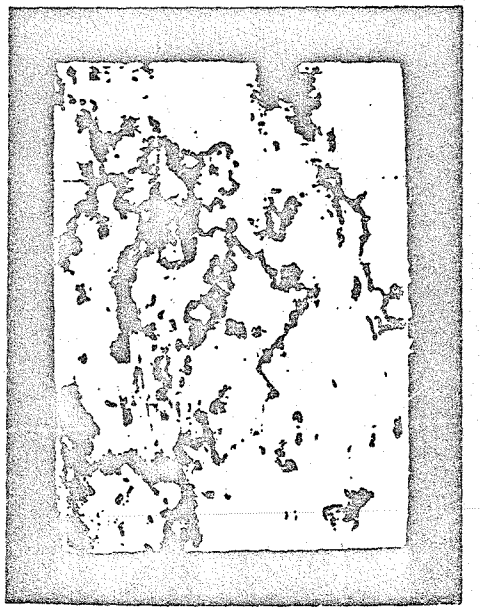

Model Position A

Hologram Number 43

44

45

46

FIGURE 13. Double Pulse Holographic Interferograms: Flow Mach Number 0.875
Pulse Spacing 100 μs. (Flow from Right to Left)

Model Position A

Hologram Number 48

49

FIGURE 14. Double Pulse Holographic Interferograms: Flow Mach Number 0.875 Pulse Spacing 30 μs. (Flow from Right to Left)

FIGURE 15. Double Pulse Holographic Interferogram: Pulse Spacing Comparison
Model Position A. (Flow from Right to Left)

APPENDIX 2

LASER HOLOGRAPHIC INTERFEROMETRY FOR UNSTEADY AIRFOIL UNDERGOING DYNAMIC STALL

(AIAA-83-0388 - January 1983)

AIAA-83-0388

Laser Holographic Interferometry for Unsteady Airfoil Undergoing Dynamic Stall

G. Lee, D.A. Buell and J. Licursi, NASA Ames Research Center, Moffett Field, CA; and J.E. Craig, Spectron Development Labs., Costa Mesa, CA

AIAA 21st Aerospace Sciences Meeting

January 10-13, 1983/Reno, Nevada

LASER HOLOGRAPHIC INTERFEROMETRY FOR AN UNSTEADY AIRFOIL IN DYNAMIC STALL

George Lee,* Donald A. Bunill† and Joseph P. Licursi‡
NASA Ames Research Center, Moffett Field, Calif.

and

James E. Craig†
Spectron Development Laboratory, Costa Mesa, Calif.

Abstract

Laser holographic interferometry was used to study a two-dimensional NACA 0012 airfoil undergoing dynamic stall. The airfoil, fabricated from graphite fiber and epoxy, was tested at Mach numbers of 0.3 to 0.6, at Reynolds numbers of 0.5×10^6 to 2.0×10^6, at reduced frequencies of 0.015 to 0.15, and at mean angles of attack of 0° to 10° with amplitudes of 10°. Density and pressure fields were obtained from dual-plate interferograms. Double-pulse interferograms, which seemed to show the wake boundaries better, were also taken. Comparisons of pressures with orifice pressures were good for the attached flow cases. For the separated flow cases, which had a vortex enbedded in the flow, the comparisons were poor. Vortices, wake structures, and the dynamic stall process can be seen by holographic interferometry.

Nomenclature

c = chord of airfoil

C_p = pressure coefficient

k = reduced frequency

L = width of test section

M = Mach number

n = refractive index of air

N = fringe number

r = recovery factor, 0.88

T = temperature

u = velocity

x,y,z = Cartesian coordinates

α = angle of attack

γ = specific heat ratio

$\Delta\phi$ = fringe shift

κ = Gladstone-Dale constant

δ = thickness of boundary layer or separated region

λ = wavelength of laser light

ρ = density

Subscripts

ad = adiabatic wall condition

e = boundary-layer edge conditions

o = reference condition

w = wall condition

Introduction

In the past few years, laser holographic interferometry has been shown to be a valuable diagnostic tool for wind-tunnel studies of steady two-dimensional flows. The entire density fields can be easily visualized and mapped quantitatively without disturbance, since only light is used to probe the flow. For the special case of infinite fringe interferograms of two-dimensional flows, the fringe lines become lines of constant density. Thus, density contours are obtained directly. With the assumption of isentropic flow, Mach number and velocity contours, which are commonly used to verify aerodynamic codes, as well as surface pressures, can be deduced from the density data. Other aerodynamic parameters of interest, such as shock waves, boundary layers, wakes, regions of separated flow, and the shedding of large scale vortices, can also be visualized using this technique.

Because of the success of laser holographic interferometry for steady two-dimensional flows, an experiment was designed to determine the feasibility of the technique for application to unsteady two-dimensional flows. For this experiment, the unsteady flow over an airfoil undergoing dynamic stall was considered since the unsteady flow effects are large. Many different types of flows occur as the airfoil goes through an oscillation. At low angles of attack, the flow is attached on the upper surface, but as the angle of attack is increased, the flow begins to separate. Small vortices appear near the onset of stall and a large dynamic-stall vortex sheds across the airfoil during deep stall. Then, as the airfoil goes through decreasing angles of attack, there is a complex reattachment process.

Previous flow visualization studies of airfoils undergoing dynamic stall have been made in both air and water. The smoke technique[1] has been used in air to visualize the streamlines, the vortices and the flow processes occurring around an airfoil as it goes through dynamic stall. Tufts, attached to the airfoil, have also been used to observe the flow-reversal process on airfoils. Similarly, dyes and polystyrene beads,[2] air bubbles,[3] and hydrogen bubbles,[4] have been used in water tunnels to make the

---

*Assistant Chief, Aerodynamics Research Branch. Member AIAA.
†Research Scientist.
‡Technician.

flow visible. The bubbles, bead, and hydrogen methods show the smaller vortices quite well, and the smoke and dye methods show the larger scale flow structures, such as the dynamic stall vortex. The main drawback of all these methods is that they are qualitative in nature. One of the many advantages of laser holographic interferometry for studying dynamic stall and other unsteady flows is that it is a quantitative measurement technique. Short laser pulses (of the order of nanoseconds) can freeze unsteady flow patterns for subsequent quantitative analysis. Moreover, the technique is very sensitive, and small density variations can be measured. In the present experiment, an existing laser holographic interferometer was synchronized to an oscillating airfoil to demonstrate laser holographic interferometry as both a quantitative and qualitative visualization technique for unsteady two-dimensional flows.

Experiments

Model

The two-dimensional airfoil model tested was a nominal NACA 0012 section with a 15.24-cm (6.00-in.) chord. In order to have a light, strong structure suitable for efficient oscillatory motion, the airfoil was fabricated from 20 plies of graphite tape impregnated with epoxy resin over a balsa wood core. The resulting surface had the smoothness of a polished metal surface; it was, however, somewhat thicker than planned, corresponding more nearly to a 12.5% section instead of the nominal 12%. See Table I for the actual airfoil coordinates.

The airfoil span was 61.0 cm (24.0 in.); between the glass windows of the test section with a gap at each end of 1 mm (0.04 in.) or less. The wing was mounted in the windows by steel stubs which rode in needle bearings. All metal parts were kept as small as possible to reduce the inertial loads. The wing was pitched about the quarter-chord axis by oscillating the driving arm, through an eccentric, with a 110-hp, variable-frequency, electric motor, as shown in Fig. 1. With this linkage, it was relatively easy to adjust the mean angle of attack, but a lengthy eccentric replacement was required to change amplitude. The motor was selected because of its large inertia, which minimized the effect of aerodynamic forces on the airfoil motion, and not because of its power rating, which greatly exceeded that required.

Spherical wing-window bearings were used to keep wing-bending from imposing moments on the glass, and the driving arm was attached through a universal-type joint. It was, therefore, necessary to restrain the end of the driving arm in a phenolic laminate guide. Although there were some maintenance difficulties with the bearings and guide, the primary weakness in the model was subsequently found to be the joint between the steel stub and the carbon epoxy composite. A sketch of the wing is shown in Fig. 1b. The bonding at the joint on the nondriven end of the airfoil separated from the stainless steel stub (despite etching) after approximately 5 million cycles, 3 million of which occurred under significant aerodynamic loading.

Airfoil, Phase and Position

A mechanical indication of phase was obtained from a segmented disk bolted onto the motor shaft. The disk pattern, consisting of one white segment in the inner track and 100 segments in the outer track, can be seen in Fig. 1. The intention was to have a positive indication of airfoil position versus time, whether or not the motor maintained a steady rotation. The segments on each track were transformed into electrical pulses by focusing the light from light-emitting diodes onto the disk and back onto photodetectors. After shaping, the pulses were then used to trigger data sampling. The primary problem with the system was an occasional loss of signal caused by losing the focus of the light-emitting diodes when the disk vibrated at certain of the higher rotational speeds.

The airfoil position was also determined from a rotary transformer which was mechanically coupled to the airfoil just outside the test-section window. The unit can be seen in Fig. 1, with its mounting bracket partially obscuring the driving arm. The position signal was amplified and recorded on the same devices as the pressure transducers described below.

Pressures

Instantaneous pressures on the wing were measured with absolute-pressure, high-response transducers. The transducers, 1.3 mm (0.052 in.) in diameter, were mounted in plastic tubes under the composite skin and connected to the surface through 0.76 mm (0.030-in.) orifices. Nine transducers were installed in each surface.

The transducer signals were processed by a balancing circuit and a dc amplifier; they were then routed to monitoring circuits, a minicomputer, an analog FM tape recorder, and to an oscillograph. The wing pressure signals were also passed to summing amplifiers for an on-line indication of lift and pitching moment.

Tests

The model was tested at Mach numbers of 0.3, 0.4, 0.5, and 0.6 at chord Reynolds numbers of 2×10^6. Reynolds numbers down to 0.5×10^6 were also tested. Tests with the airfoil stationary were conducted at angles of attack from -25° to +20° at 2.5° intervals, except at the stall angle, where the wing (restrained at one end only) fluttered. Oscillatory tests were conducted with mean angles of attack of 5° and 10° at an amplitude of 10° at frequencies up to 36 Hz.

Holographic Interferometry

A basic description of holographic interferometry is given in many textbooks, for example, in Vest.[5] In interferometry, two or more waves are superimposed, and the resulting constructive and destructive interference causes bright and dark fringes, respectively. Holographic interferometry allows the storage of two waves separated in time to be superimposed in reconstruction. The two waves can be stored on a single hologram (double-pulse holographic interferometry), or on two separate plates (dual-plate holographic interferometry). The double-pulse technique is easily accomplished, but it is less flexible because the fringe spacing is

fixed. The superimposed reconstruction waves are viewed directly and then photographed.

The double-pulse technique was used to study unsteady motions, and the information recorded is the change in densities which occurs during the time between the laser pulses. The data are qualitative in this case, because no reference density condition was available. The dual-plate technique is more difficult, but it is much more flexible than the double-pulse technique. It is necessary to use this method when quantitative flow-field data are required. In using dual-plate holography, a reference exposure is recorded with no flow in the test field on the first film plate. Another exposure is recorded at test conditions on the second film plate. A special two-plate carrier used in the reconstruction system allows adjustment of the first film plate position with respect to the second film plate. When the plates are repositioned correctly, the reconstructed wave fronts interfere to form a fringe pattern. If both holograms were recorded in the absence of aerodynamic flow, the reconstructed interferogram should exhibit broad fringe spacings, with only a few fringes in the field owing to slight misalignment and optical imperfections. When one of the holograms is recorded in the presence of aerodynamic flow the fringes, being contours of constant phase shift, represent constant-density contours in the special case of two-dimensional flows.

The equation for the fringe shift is

$$\Delta\Phi(x,y) = \int_0^L [n(x,y) - n_o]dz = N\lambda \qquad (1a)$$

and for two-dimensional flows, the change in index of refraction is

$$n(x,y) = n_o + \frac{N\lambda}{L} \qquad (1b)$$

Using the Gladstone-Dale equation that relates the refractive index of air to the density, the density can be shown to be

$$\rho(x,y) = \frac{N\lambda}{kL} + \rho_o \qquad (1c)$$

Once a particular fringe and its corresponding reference density are identified, the entire flow field is determined.

The laser holographic interferometer at the 2- by 2-Foot Transonic Wind Tunnel at Ames Research Center has been described by Craig.[6] It is an off-axis system which incorporates a modern, 10-pps Nd:YAG pulsed laser; the laser provides reliable operation and is easy to align. A sketch of the interferometer with photographs of the laser, transmitting and receiving optics, and the holographic plate is shown in Fig. 2. For the dynamic stall experiment, or for any unsteady flow applications, it is necessary to synchronize the laser pulse to an external event. The internal oscillator of the laser was replaced by an external one. If the external oscillator frequency is not within the 8-12-Hz range required for thermal equilibrium in the Nd:YAG rod, the source frequency must be multiplied or divided in a synchronous manner by integer amounts to achieve the proper frequency range. In this experiment, the airfoil was driven in pitching oscillation at frequencies from 10-40 Hz. For the airfoil images to coincide in the infinite fringe interferograms, both reference and object hologram must be recorded at the same airfoil position. The laser triggering was synchronized to an encoder signal from the airfoil pitch drive motor. Using an adjustable time delay, flow-on and flow-off holograms were recorded at repeatable airfoil positions throughout the oscillation cycle for the range of frequencies considered.

Reconstruction of Dual-Plate Interferograms

A typical reconstruction sequence of dual-plate interferograms to the final desired infinite-fringe mode is shown in Fig. 3. This is for a symmetric NACA 0012 airfoil at $\alpha = 1°$. At the first stage of reconstruction (Fig. 3a), the object and reference plates are placed in the dual-plate holder and the airfoil and oscillating mechanism, that is, the dark shapes, are superimposed. The large number of fringes is typical of finite fringe interferograms. The second stage involves small movements of one plate with respect to the other to both minimize the number of fringes, and to achieve a fringe pattern based on a prior knowledge of the aerodynamics. In this case, the symmetric airfoil at $\alpha = 1°$ should give a fringe pattern that is nearly symmetric to the horizontal plane of symmetry of the airfoil. The second stage interferogram (Fig. 3b), shows fair symmetry except for the one fringe that crosses the airfoil at about 75% chord. It is further noticed that there are a number of vertical fringes behind the airfoil; these fringes indicate a change in density which should not occur. The final stage consists of minor adjustments to get rid of these vertical fringes and to minimize the number of fringes in the outer regions surrounding the airfoil, since these regions should have the smallest density gradients. Figure 3c shows the final infinite fringe interferogram used for data analysis.

Results

A typical sequence of infinite fringe interferograms of the airfoil going through one cycle of oscillation is shown in Fig. 4. Surface pressures, boundary layer, and wake profiles were measured from interferograms at a Mach number of 0.4, Reynolds number of 2×10^6, and a reduced frequency of 0.1. The dynamic-stall process, with the formation of the vortex, its shedding, and the reattachment of the flow, can also be determined.

Figure 5 shows the comparison of surface pressures as measured from the interferograms and pressure orifices at three points of the cycle: an attached flow, a separated flow, and a reattaching flow. The digitizing of the fringes was done using an electronic digitizer connected to a minicomputer. This made the tedious digitizing task easier; a pressure distribution plot could be obtained in 15 min or less. Since interferometric data were available for the rear half of the airfoil, the pressure distributions of Wood[7] were added for qualitative comparison since Wood's data were obtained at slightly different test conditions.[1] The agreement of the interferometric and orifice data is about 1% for the attached flow and reattaching flow cases. For the separated flow cases, the agreement is poor, and the interferometric technique for measuring surface pressures apparently does not work. Examination of the interferograms reveals that large vortices are being shed in a highly separated flow. This means that pressure gradients normal to the stream direction can exist, which

invalidates one of the basic assumptions used in obtaining surface pressures by interferometry. This result is different from previous results[8] in separated flow. Obviously, a method that can account for the effects of the vortex must be developed before pressures can be obtained by interferometry.

Boundary-layer and separated flow thickness were measured over the rear half of the airfoil. The leading edge of the airfoil can be seen (Fig. 4) but most of the front half of the airfoil is obscured by the oscillating apparatus. The boundary layer and its edge can be easily defined. For example, as seen in Fig. 4, the fringes within the boundary layer are quite thin and closely spaced because of the large density gradients within the boundary layer. Another factor that helps in defining the boundary layer is that the density gradients in the outer inviscid region are approximately normal to the density gradients in the boundary layer. This results in a sharp break in the fringes at the edge of the boundary. Using the above criteria, the boundary-layer thickness and the thickness of the separated flow region were determined. The thickness of the separated flow region was not as well defined and could be off several fringes in the infinite interferograms. Therefore, the double-pulse interferograms, which gave better definition of the edge of the separated flow, were used for separated flows.

A plot of the boundary layer and separated-flow thickness of the 95% chord station for one complete cycle of oscillation from -5° to 15° is presented in Fig. 6. At the start of the cycle, the boundary-layer thickness is about 0.7% of the chord, and it grows with increasing angle of attack to nearly 5% of chord at the onset of stall at about 14.0°. Up to this angle, the boundary-layer velocity profiles do not show any separated flows. At 14.0°, the layer grows to 11% of the chord and there is a small vortex near the midchord of the airfoil (see Fig. 4, $\alpha = 14.0°$). At angles slightly above 14°, stall occurs, the flow separates, and a large vortex sweeps over the top of the airfoil. This seems to indicate a trailing-edge-type stall. This result is based on the observation of many interferograms. After stall, the flow thickness is nearly 60% of the chord. At this point in the cycle and with decreasing angles, the separated-flow region decreases until complete reattachment occurs at an angle of attack of about -1°. Examination of the interferograms indicates that the large dynamic-stall vortex has been replaced by several smaller ones. These vortices are continually swept downstream and disappear when reattachment occurs.

Velocity profiles at three chordwise stations and slightly into the wake were measured for the attached-flow, separated-flow, and reattaching-flow cases. Velocity profiles were derived from the density, using the Crocco equation,[9]

$$\frac{\Gamma}{\Gamma_e} = 1 + r\,\frac{\gamma - 1}{2}\,M_e^2\left[1 - \left(\frac{u}{u_e}\right)^2\right] + \frac{T_w - T_{ad}}{T_e}\,(1 - u/U_e) \qquad (2)$$

and the perfect gas law. Constant pressure in the boundary layer was also assumed in the Crocco derivation. Figure 7 shows the velocity profiles data from the interferograms, and Carr's flow model for attached and separated flow. The models from Carr et al. were based on experimental measurements such as smoke data. Overall, the interferometric profiles are similar to those of the model. (It is assumed that the reattaching flow is an attached flow case.) A closer examination of the interferometric data from the midchord to about 85% chord for attached and reattaching cases identifies two problems: 1) the velocity does not go to zero at the surface, as expected; and 2) the large velocity gradient at the surface that is typical of turbulent boundary layers is not seen. The cause of both problems is the bending of the airfoil caused by aerodynamic forces; the bending blocks the fringes near the surface. For a turbulent profile, there should be a large number of fringes near the surface because of the large density gradients. This problem disappears in the wake and is not as crucial near the trailing edge, because the gradients there are mild and only one or two fringes are lost because of model bending.

Velocity profiles at the midchord and the near-wake determined by laser velocimetry by Owen[10] and by interferometry agreed very well for the attached flow and reattaching flow (see Figs. 8a and 8c). It is noted that interferometry gives an instantaneous point in the cycle and that laser velocimetry gives an average over many cycles. For the separated flows (Fig. 8b), the agreement between the two methods is poor. Again, as in the calculation of surface pressures, the basic assumption of zero pressure gradients in the normal direction, used in deriving the Crocco equation, was violated. Another basic assumption, that of constant total enthalpy, was also violated as a result of the unsteady flow.

A typical double-pulse interferogram is presented in Fig. 9. The separated flow region and the wake exhibit large numbers of fringes because of density fluctuations that occur within the time of the laser pulses — about 0.1 msec. Outside the separated region and the wake, the density remains essentially constant during this time; therefore, there are very few fringes in these regions. As a result, the boundaries of the wake and separated regions are much better defined in the double-pulse interferograms. Note that double-pulse data are qualitative in nature.

Interferograms were also taken at a lower Reynolds number (1×10^6). As expected, the number of fringes is reduced. According to Eq. 1c, the reduction in fringes is directly proportional to the magnitude of the density. As seen in Fig. 10, the boundary layer, separated flow region, and wake structure are well defined. The lack of fringes would affect the accuracy, the velocity profiles, and further reductions in densities could affect the usefulness of the interferometric technique.

Summary

Laser holographic interferometry was tried as a nonintrusive diagnostic tool for studying unsteady two-dimensional flows. A NACA 0012 airfoil was tested, while undergoing dynamic stall, over a range of Mach numbers of 0.3 to 0.6, Reynolds numbers of 0.5×10^6 to 2×10^6, and at reduced frequencies of 0.015 to 0.15. It was found that both quantitative and qualitative data could be obtained by the technique. Surface pressures on the airfoil can be measured to within 1% of those measured with orifices and pressure transducers when the flow is

attached. Velocity profiles were measured near the wake region, and they compared very well with laser velocimeter data for attached flows. For separated flows with large-scale vortices, densities can be measured, but pressures and velocities cannot be deduced with the assumption of constant pressure gradient in the normal direction. The sensitivity of the interferograms was good at a Mach number of 0.4 and a Reynolds number of 4×10^6/ft; the sensitivity worsened at smaller Mach numbers and Reynolds numbers, and improved at larger ones.

References

[1]Carr, L. W., McAlister, K. W., and McCroskey, W. J., "Analysis of the Development of Dynamic Stall Based on Oscillating Airfoil Experiments," NASA TN D-8382, 1977.

[2]Werle, H., "Hydrodynamics Flow Visualization," in Annual Review of Fluid Mechanics, VS, M. VanDyke and W. G. Vincenti, Eds., Annual Review Inc., Palo Alto, Calif. 1973.

[3]Werle, H., "Flow Visualization Techniques for the Study of High Incidence Aerodynamics," Von Kármán Institute, Lecture Series 121, AGARD, Langley Research Center, NASA, Mar. 1981.

[4]McAlister, K. W. and Carr, L. W., "Water Tunnel Visualization of Dynamic Stall," Transactions of the American Society of Mechanical Engineers, Vol. 101, 1979.

[5]Vest, C. M., Holographic Interferometry, John Wiley, New York, 1979.

[6]Craig, J. E., "Operating Manual Holographic Interferometry System for 2- by 2-Foot Transonic Wind Tunnel," NASA CR-166344, 1981.

[7]Wood, M. E., "Results of Oscillatory Pitch and Ramp Tests on the NACA 0012 Blade Section," Aircraft Research Association Limited Memo. 220, Bedford, England, 1979.

[9]Johnson, D. A. and Bachalo, W. D., "Transonic Flow about a Two-Dimensional Airfoil — Inviscid and Turbulent Flow Properties," AIAA Paper 78-1117, Seattle, Wash., 1978.

[9]Schlicting, H., Boundary Layer Theory, McGraw-Hill Book Co., New York, 1960.

[10]Owens, F. K., private communication, Complere Inc., 1982.

Table 1 Theoretical and measured airfoil coordinates

Chord Station %	Specified thickness % of chord	Measured thickness % of chord Upper	Lower
0.78	1.52	1.44	1.82
1.77	2.23	2.15	2.53
3.97	3.27	3.14	3.52
8.22	4.35	4.31	4.65
17.30	5.55	5.58	5.84
29.28	6.00	6.07	6.24
46.42	5.50	5.64	5.60
63.18	4.29	4.42	4.38
75.13	3.15	3.27	3.15
87.47	1.76	1.92	1.72

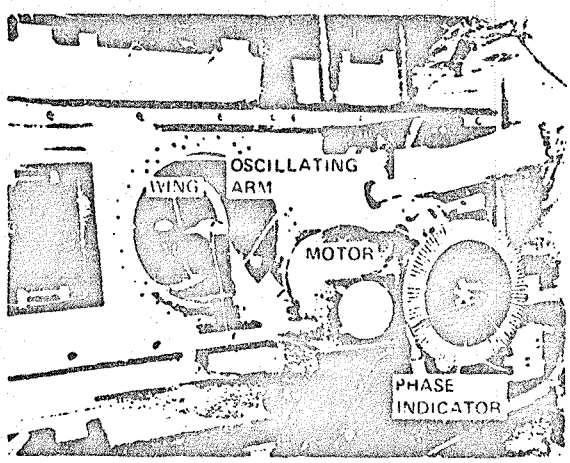

Figure 1a.- Photograph of wind tunnel, wing, and oscillating mechanism.

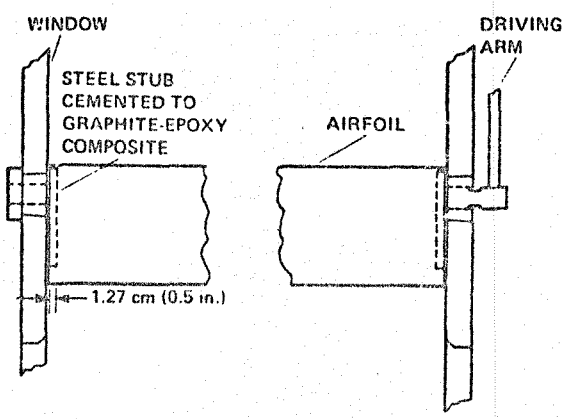

Figure 1b.- Sketch of airfoil mounting.

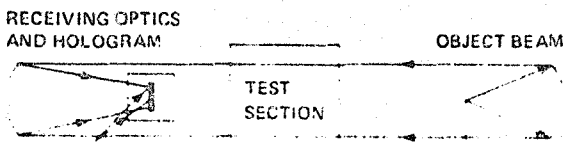

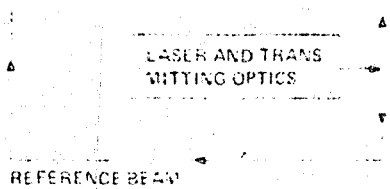

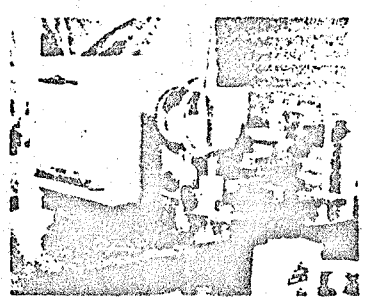

RECEIVING OPTICS AND HOLOGRAM

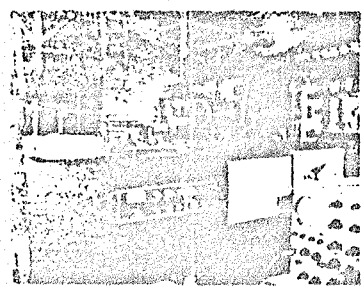

LASER AND TRANSMITTING OPTICS

Figure 2.- Two- by two-foot interferometer.

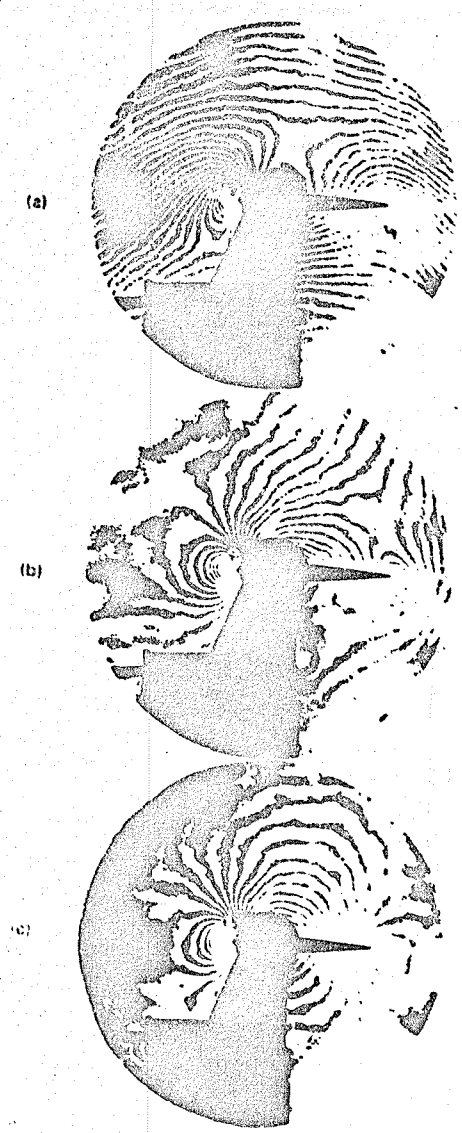

Figure 3.- Reconstruction process of infinite fringe interferograms. a) Initial alignment; b) intermediate alignment; c) final alignment.

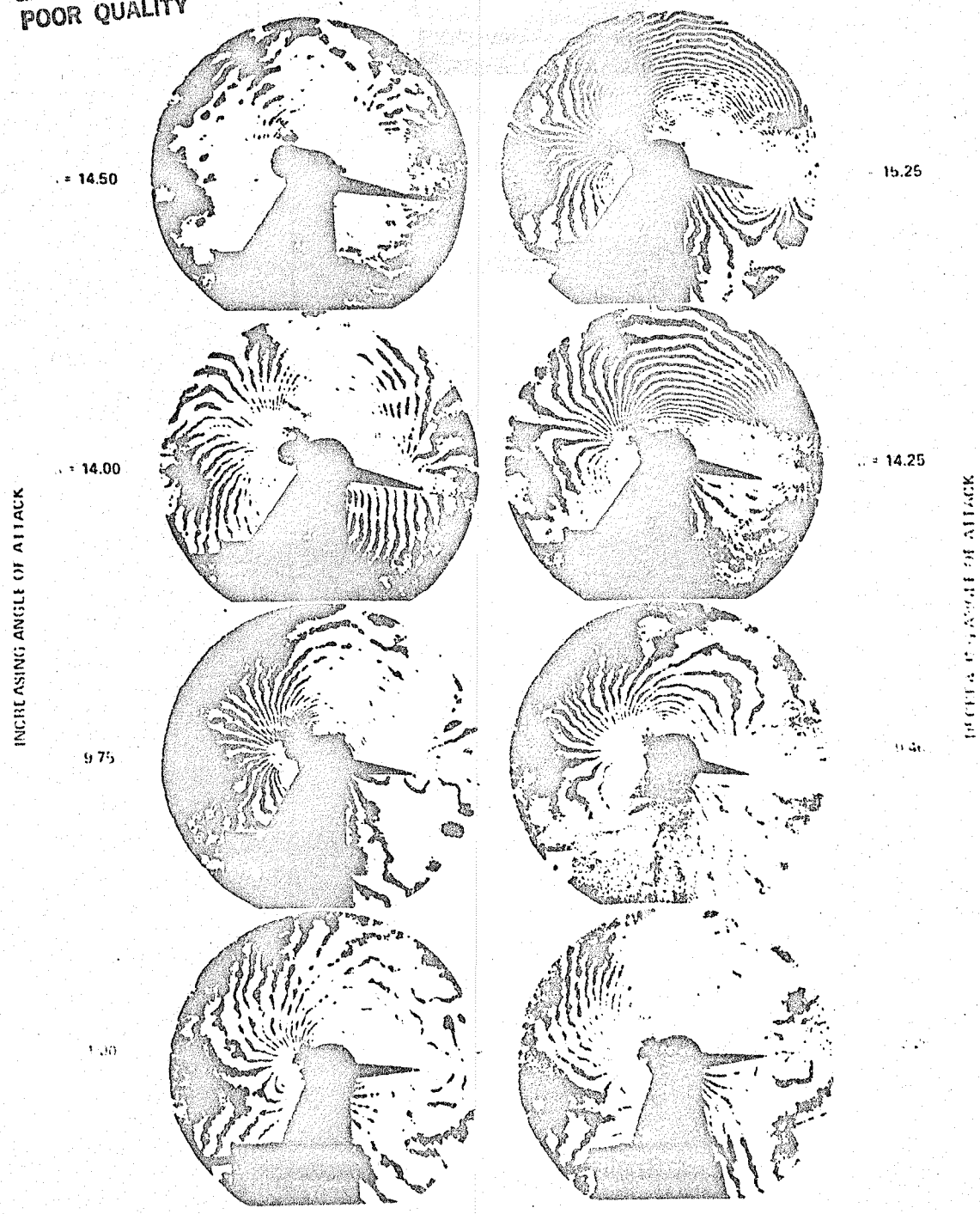

Figure 4.- Sequence of interferograms showing the airfoil going through dynamic stall.

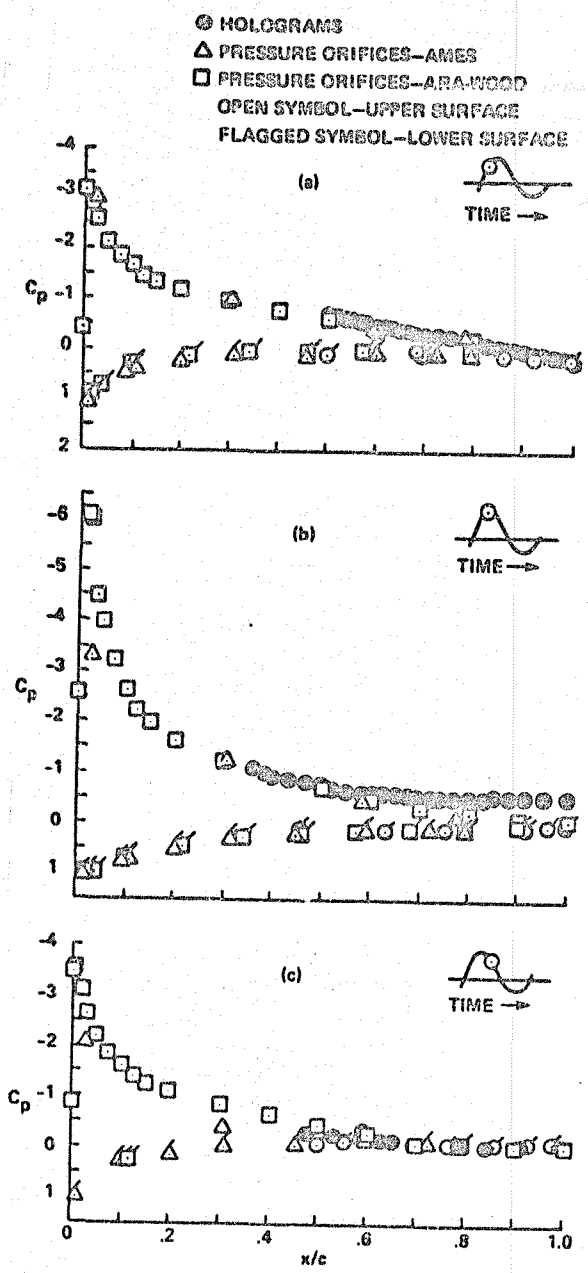

Fig. 5 Comparison of surface pressures from interferograms and orifices: M = 0.4, Re = 2×10^6, k = 0.1. a) Attached flow, $\alpha = 9.13°$; b) separated flow, $\alpha = 14.39°$; c) reattaching flow, $\alpha = 9.46°$.

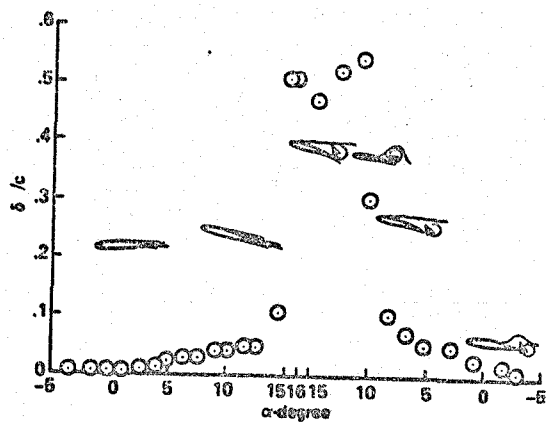

Fig. 6 Boundary-layer thickness and shear-layer thickness as airfoil goes through dynamic stall; M = 0.4, Re = 2×10^6, k = 0.1, x/c = 95%.

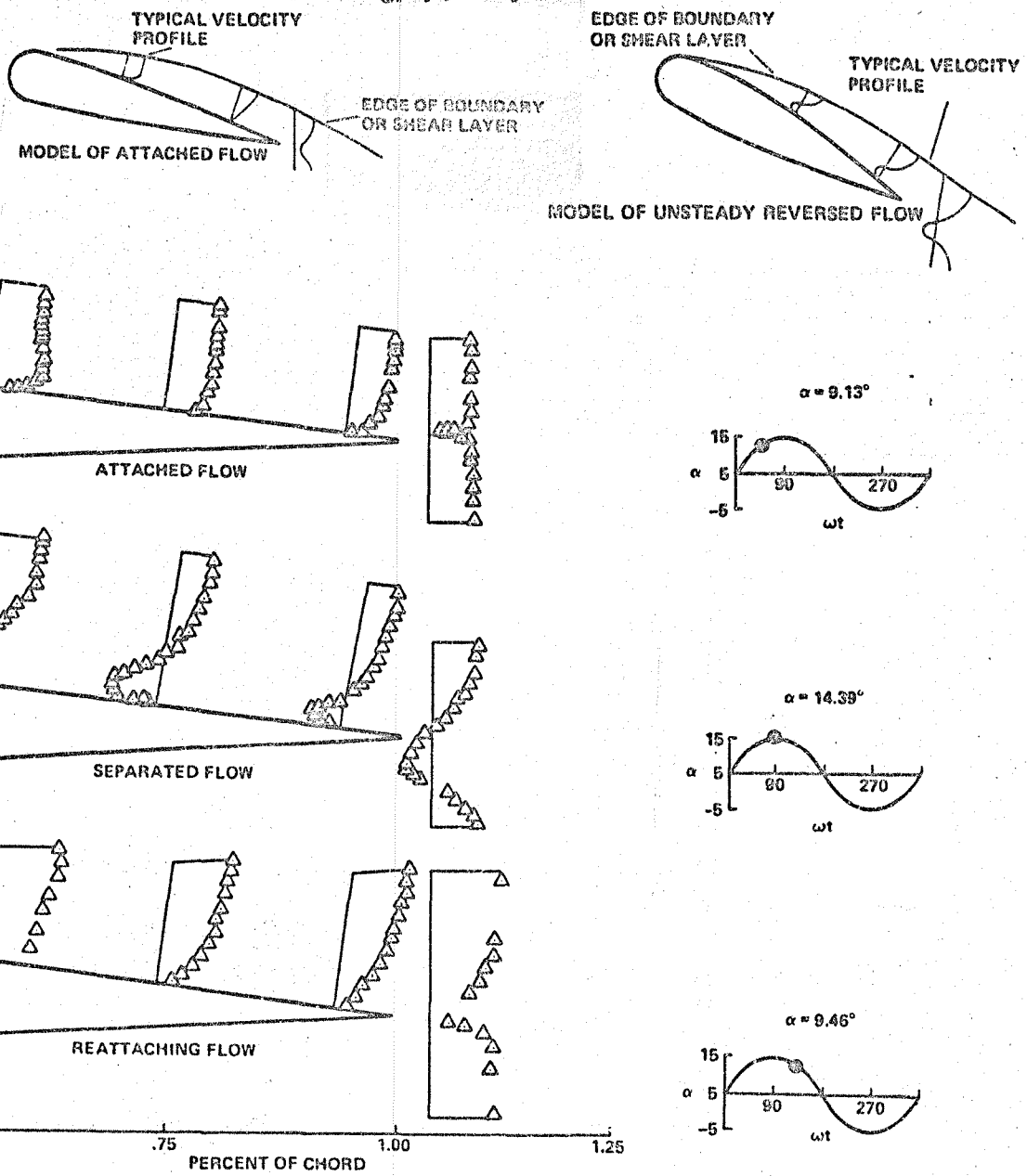

Figure 7.- Interferometric velocity profiles: M = 0.4, Re = 2×10^6, k = 0.1.

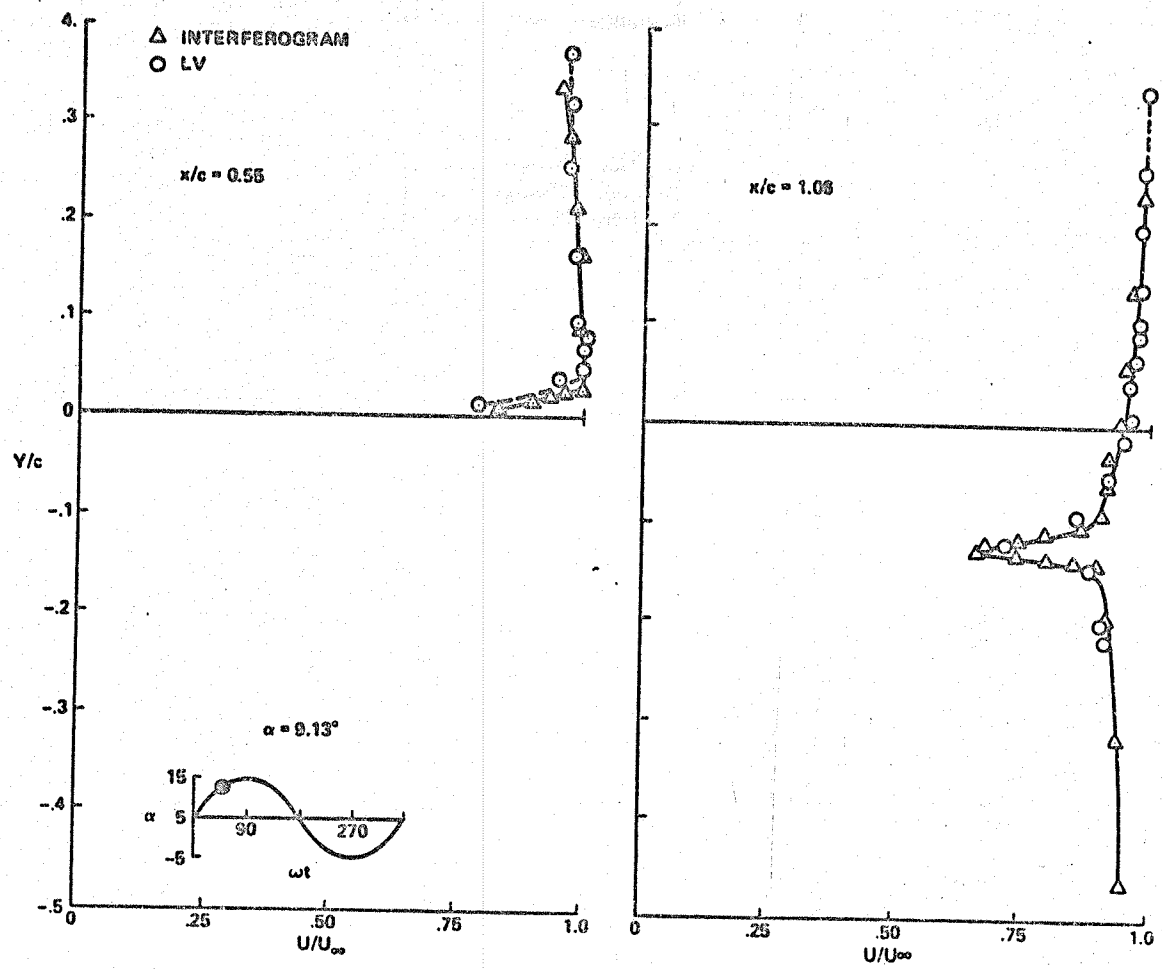

a) Attached flow

Fig. 8 Comparison of velocity profiles with laser velocimetry data.

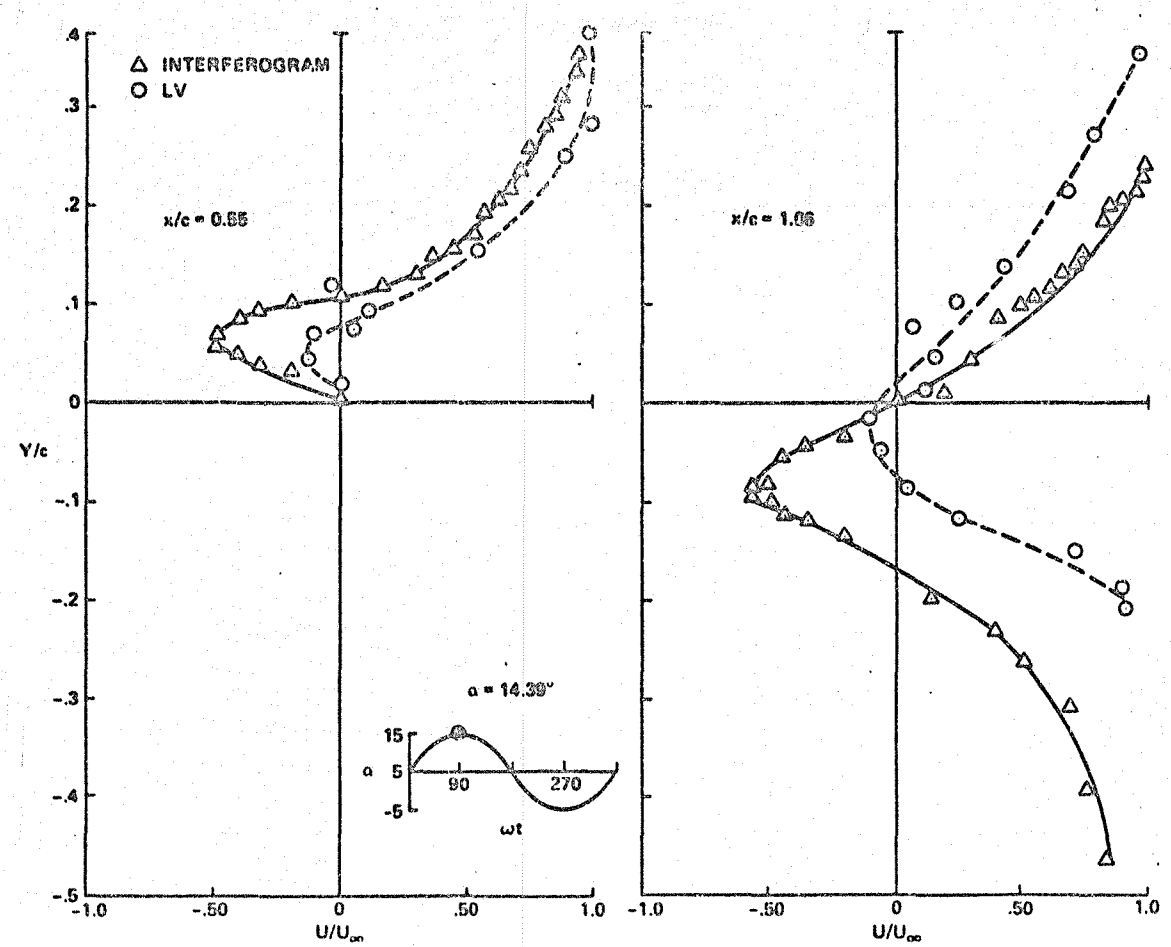

b) Separated flow

Fig. 8 Continued.

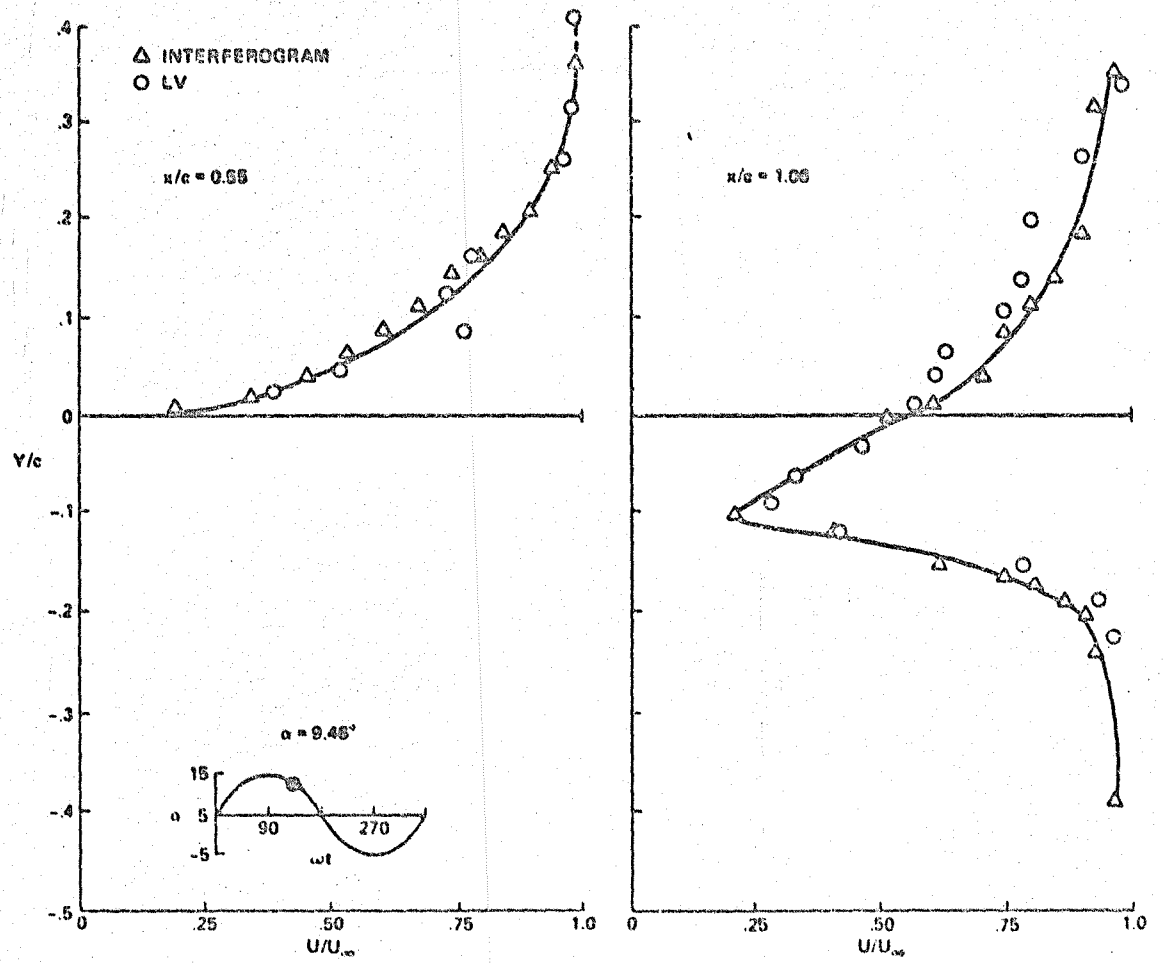

c) Reattaching flow: $M = 0.4$, $Re = 2 \times 10^6$, $k = 0.1$

Fig. 8 Concluded.

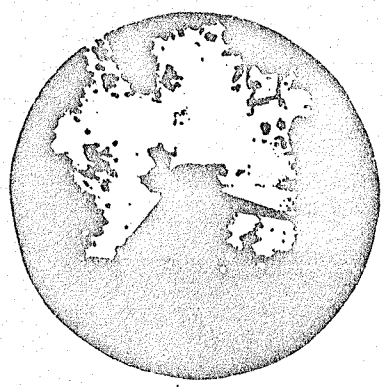

Fig. 9 Double pulse interferogram, M = 0.6, Re = 4 × 10^6, α = 15.1°, k = 0.05.

(a)

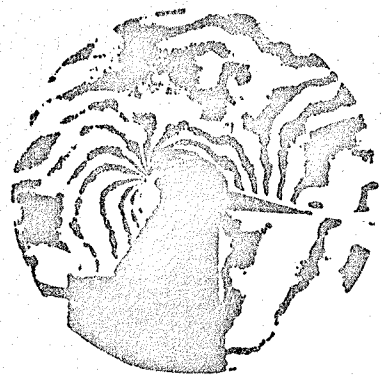

a) Re = 1 × 10^6, M = 0.4, α (ascending) = 10°, k = 0.1.

(b)

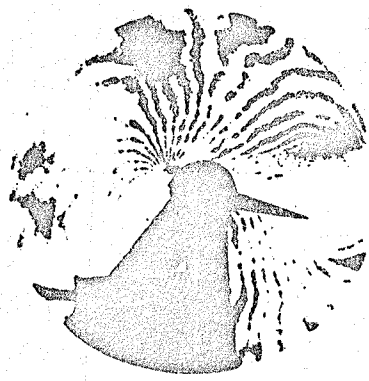

b) Re = 1.5 × 10^6, M = 0.6, α (ascending) = 15°, k = 0.05.

Fig. 10 Interferograms at lower Reynolds number.

END

DATE

FILMED

AUG 23 1983

End of Document